

TALLINN UNIVERSITY OF TECHNOLOGY  
DOCTORAL THESIS  
1/2019

# **On Statistical Topography of Self-Affine Sets**

INDREK MANDRE



TALLINN UNIVERSITY OF TECHNOLOGY

School of Science

Department of Cybernetics

The dissertation was accepted for the defence of the degree of Doctor of Philosophy (Applied Mathematics) on October 3<sup>rd</sup>, 2018

**Supervisor:** Jaan Kalda, PhD  
Department of Cybernetics, School of Science  
Tallinn University of Technology  
Tallinn, Estonia

**Opponents:** Alex Hansen, PhD  
Department of Physics  
Norwegian University of Science and Technology  
Trondheim, Norway

Els Heinsalu, PhD  
National Institute of Chemical Physics and Biophysics  
Tallinn, Estonia

**Defence of the thesis:** January 15<sup>th</sup>, 2019, Tallinn

**Declaration:**

*Hereby I declare that this doctoral thesis, my original investigation and achievement, submitted for the doctoral degree at Tallinn University of Technology, has not been submitted for any academic degree elsewhere.*

Indrek Mandre

---

signature



European Union  
European Social Fund



Investing  
in your future

Copyright: Indrek Mandre, 2019

ISSN 2585-6898 (publication)

ISBN 978-9949-83-373-3 (publication)

ISSN 2585-6901 (PDF)

ISBN 978-9949-83-374-0 (PDF)

TALLINNA TEHNIKAÜLIKOOL  
DOKTORITÖÖ  
1/2019

# **Eneseafiinsete hulkade statistilisest topograafiast**

INDREK MANDRE



---

## CONTENTS

---

LIST OF PUBLICATIONS	6
1 INTRODUCTION	7
2 FRACTALS, SELF-SIMILARITY AND PERCOLATION	10
2.1 Self-similar processes . . . . .	12
2.2 The spectral connection . . . . .	15
2.3 Self-affine fractals and fractal dynamics . . . . .	18
2.4 Percolation and critical phenomena . . . . .	20
2.5 Correlated percolation . . . . .	21
2.6 Scaling of two-dimensional correlated percolation clusters . . . . .	23
3 ON SIMULATION OF RANDOM PROCESSES	25
3.1 Random number generation . . . . .	25
3.2 Stationary Gaussian random processes . . . . .	27
3.3 Fractional Brownian motion and surfaces . . . . .	29
3.4 Direct use of fast Fourier transform . . . . .	30
3.5 Use of spectral self-similarity and division of scales . . . . .	33
3.6 Other methods and references . . . . .	34
3.7 Mapping of a random potential into land and sea . . . . .	34
4 CALCULATION OF SCALING EXPONENTS	36
4.1 The wavelet method . . . . .	38
4.2 Fractal scaling exponents and finite size effects . . . . .	40
5 CONCLUSIONS AND FURTHER WORK	43
BIBLIOGRAPHY	47
ACKNOWLEDGMENTS	54
ABSTRACT	55
KOKKUVÖTE	57
APPENDIXES	59
PUBLICATION I . . . . .	61
PUBLICATION II . . . . .	71
PUBLICATION III . . . . .	79
CURRICULUM VITAE	85
ELULOOKIRJELDUS	88

---

LIST OF PUBLICATIONS AND THE AUTHOR'S ORIGINAL  
CONTRIBUTION TO SCIENCE

---

P1 I. Mandre, J. Kalda. Monte-Carlo study of scaling exponents of rough surfaces and correlated percolation. *The European Physical Journal B*, 83(1):107-113 (2011).

Monte-Carlo calculation of the fractal dimensions of the two-dimensional percolation cluster hull and the unscreened perimeter for the universality class of correlated percolation and rough surfaces. A random potential with power law power spectrum  $\mathcal{S}[X](\omega) \propto \omega^{-2H-2}$  is mapped into percolation clusters and scaling exponents are calculated in the parameter range  $-3/4 \leq H \leq 1$ .

P2 I. Mandre, J. Kalda. Efficient method of finding scaling exponents from finite-size Monte-Carlo simulations. *The European Physical Journal B*, 86(2):56 (2013).

Contribution to the testing, verification and publishing of a general method to calculate the scaling exponents of fractal structures. The method compensates for a common form of finite-size effects and provides clear rules for its application and for determining the validity of the assumptions and the result.

P3 I. Mandre, J. Kalda. Intersections of moving fractal sets. *EPL (Europhysics Letters)*, 103(1):10012 (2013).

Discovery that the mass of finite intersections of moving fractals as a function of relative movement distance is self-affine and the derivation of the analytical relation for its scaling exponent.

The publications can be found at the end of the thesis. From here on they are referenced correspondingly as [P1], [P2] and [P3].

---

## INTRODUCTION

---

“Clouds are not spheres, mountains are not cones, coastlines are not circles, and bark is not smooth, nor does lightning travel in a straight line.” – Benoit B. Mandelbrot [1].

**T**HE SUBJECT MATTER of this thesis concerns with trying to make sense of the chaotic and random physical world. Classical physics often reduces practical problems into the most simple models – as example, planets and asteroids orbiting the sun can be treated as point masses and their trajectories predicted by integration of the Newton’s laws – basic equations of motion. The problem of the movement of planets is seemingly solved. While the equations are known, the integration and method of calculation is understood and trivial, the resulting trajectories can be incredibly complex and in extreme cases (unstable planetary models) may look, to a human, completely chaotic. Even our Solar system has chaotic properties [2, 3]. It has been found that this is often the property of nonlinear systems of differential equations – a set of equations with reasonable parametrisation can produce deterministically chaotic results that have fractal properties [4]. While differential equations offer a precise representation of local changes at small scales, they do not provide much insight into the the resulting large-scale or long-term structures.

Complex large scale phenomena can also arise from interactions at small scales. Take the percolation problem. Here, randomly distributed minerals in rock formations form large fractal clusters – a web of connected resources. This is of importance in hydrology and oil pumping [5]. In the study of ferromagnetism, fractal clusters of atoms with similar spin (called domains) form below the Curie temperature [6]. It turns out that near their critical points these very different physical phenomena can be characterised by the same laws.

Another area of interest is turbulent flow – here, energy applied at the largest length scales divides into flows of smaller and smaller scale until reaching the point of dissipation due to viscosity. The energy spectrum at different length scales of the turbulent flow follows a power law, this is called the Kolmogorov

energy spectrum [7]. From this, one can derive that weak-turbulent gravity waves produce a random surface with fractal properties [8, 9]. As we will see, isolines of the stream function of two-dimensional turbulent flow can be connected back to the percolation problem and are of importance in understanding diffusion and mixing [10]. Random surfaces or potentials in different phenomena can be described by the same laws; another example would be random deposits of silicate – they yield a fractal surface [11]; fractals can be found in the shape of mountain ranges and coastlines [12, 13].

Small scale or local interactions yield complicated fractal structures at wide range of scales. These vast structures interact with each other producing new phenomena. Precipitation can be characterised as a spatial-temporal fractal [14, 15] and in case it interacts with the fractal structure of a river basin, the flow rate of the river can be described as the intersection between these two structures. Hurst, in his study of the river Nile, showed that its flow rate is correlated at very long timescales that can be described by a power law [16], and so has fractal properties.

But how to describe this chaos and randomness that can be found everywhere? Every physical system and every model is different and unique. It is of great interest to find common properties across different systems, fundamental laws that span different areas of physics, laws that describe and explain this complexity.

The work described in this thesis studies these kind of properties: in publication [P1], we calculate the fractal dimensions of two-dimensional correlated percolation clusters (the hull and the unscreened perimeter); we develop a method to efficiently and accurately calculate these exponents using Monte-Carlo methods in paper [P2]; and finally, we look into the moving intersections of physical fractal sets in paper [P3].

In the following chapter, we start off by defining what we mean by a fractal and introduce the fractal dimension. In sections 2.1-2.2 we give a mathematical definition of self-similar random processes, describe the commonly used models, investigate their spectral properties and show how they form fractal structures. In section 2.3 we describe the work done in [P3] by connecting the dynamic intersections of fractals to self-similar processes. In sections 2.4-2.5 we define the percolation problem, how it relates to critical phenomena and the concept of universality, and how self-similar processes can be mapped into the correlated percolation problem; in section 2.6 we describe the work done in [P1] – calculation of the scaling exponents of two-dimensional correlated percolation clusters (the cluster hull and the unscreened perimeter).

For many properties investigated there is no known analytical form or they are only known at limited points in the parameter space; sometimes the derived

values and relations are based on conjecture and circumstantial evidence. Due to this the research relies heavily on Monte-Carlo calculations – this method offers a way to statistically test the results and also calculate the searched scaling exponents where analytical form is not known. The problems encountered and techniques applied for the Monte-Carlo methods, from random number generation, self-similar process synthesis to data analysis, are described in sections 3.1-4.1. And finally, in section 4.2, we describe the work done in [P2] – the method used to efficiently and accurately extract the scaling exponents from the generated percolation clusters.

Most of the work is connected to investigating statistical properties of random surfaces – this is known as statistical topography [17].

**H**OW LONG is the coast of Britain? On this seemingly simple question elaborated Mandelbrot in his seminal 1967 paper [12]. It turns out that when measuring the length of a coast  $L$  we get different results for different lengths  $\lambda$  of a measuring stick (also known as measuring by compass). It appears we can not really characterise the length of a coast with a single number. When plotting the measurements against the compass size on a log-log graph, a curve appears that is linear through many scales. From this one can conjecture the following relation [18]:

$$L(\lambda) = M\lambda^{1-D} \quad \lambda_{\min} < \lambda < \lambda_{\max}, \quad (2.0.1)$$

where  $M$  and  $D$  are constant for the given coast and  $(\lambda_{\min}, \lambda_{\max})$  specify the interval where the equation holds. It was found that  $D$  varies from place to place (ranging from 1 to 1.25), and for the west coast of Britain we have approximately  $D \approx 1.25$ .

Mathematicians have generalised the idea of dimension of a set, leading to dimension numbers that can be fractional. Suppose we have a set of points  $F$  in  $d$ -dimensional space. Kolmogorov proposed to measure the dimension number of the set  $F$  as

$$D_K = - \lim_{\lambda \rightarrow 0^+} \frac{\log N_\lambda}{\log \lambda}, \quad (2.0.2)$$

where the covering number  $N_\lambda$  is the minimum number of  $d$ -dimensional hypercubes of side  $\lambda$  needed to cover the set of points  $F$  [19]. Clearly, in 3-space primitive structures like a point, a straight line, a plane or a cube would produce integer values (correspondingly 0, 1, 2 and 3) – in these trivial cases the covering dimension  $D_K$  is equal to the topological dimension of the structure. We call structures with covering dimension different from the topological dimension as fractals.

A physical fractal is of finite size and so has a lower and upper scaling range  $(\lambda_{\min}, \lambda_{\max})$ . All the points of  $F$  fit into a single box of size  $\lambda_{\max}$ , so we have  $N_{\lambda_{\max}} = 1$ . Below that, we should have

$$N_{\lambda} \simeq \left( \frac{\lambda_{\max}}{\lambda} \right)^D \quad \lambda_{\min} < \lambda < \lambda_{\max}. \quad (2.0.3)$$

This relation is used to measure the fractal dimensions using the box counting algorithms [20]. Suppose we have a section of a curve and we cover it with boxes of size  $\lambda$ . We can estimate the total length  $L(\lambda)$  then as

$$L(\lambda) \simeq \lambda N_{\lambda} \simeq \lambda \left( \frac{\lambda_{\max}}{\lambda} \right)^D \propto \lambda^{1-D}. \quad (2.0.4)$$

This is the same analytical relation as was conjectured in equation (2.0.1) and suggests that the coast of Britain is a fractal.

Extracting a  $d$ -dimensional ball of radius  $a < \lambda_{\max}$  from the set  $F$  while fixing the box size to  $\lambda_{\min}$  gives us another scaling relation:

$$M(a) \simeq \left( \frac{a}{\lambda_{\min}} \right)^D \quad \lambda_{\min} < a < \lambda_{\max} \quad (2.0.5)$$

which can also be used to define the fractal dimension (called the mass fractal dimension). This relation is used in [P1] and [P2] to calculate the fractal dimensions of the percolation cluster hull and the unscreened perimeter. This calculation is usually complicated by the finiteness of the samples measured – the deviations from the limit to infinity are called finite size effects. A method to overcome these is the subject of [P2].

Aside from the Kolmogorov dimension (2.0.2) or the mass dimension, other definitions have been proposed. One of the mathematically more rigorous and general is the Hausdorff dimension [21, p. 31]. Fortunately, very often, and especially for physical fractals, the dimension numbers of the various definitions coincide. A rigorous treatment of the fractal dimension theory can be found in [21].

When we take an intersection of two fractal sets of points  $F_1$  and  $F_2$  with corresponding fractal dimensions  $D_1$  and  $D_2$ , the resulting set of points  $F_1 \cap F_2$  is also a fractal, with the fractal dimension of the intersection given [22] as

$$D = D_1 + D_2 - d. \quad (2.0.6)$$

It is possible to combine two fractal sets where the equation above produces a negative fractal dimension number [23]. These intersections are not fractals but rather sparse sets of points. Mandelbrot suggests to use negative values as a measure how “empty” the given set is. Potential negative fractal dimension is encountered in [P3].

While the coastlines found in nature are inherently random, one can also synthetically construct fractal structures that appear very regular and, to a human eye, appear to contain smaller and smaller copies of the base structure. This is called self-similarity. Examples of these models would be the Koch curve [24] and the Sierpiński carpet [25–27]. Self-similarity is a general property of fractals. Random fractals are also self-similar and this can be rigorously defined in terms of statistical distributions. An example of a random fractal signal  $\{t, f(t)\}$  is the fractional Brownian motion - a model for self-affine fractals, discussed in section 2.1 and used extensively in [P3]. Here, the self-similarity can be described in terms of the curve containing affine valleys and hills, on top of which there are smaller valleys and hills, and so on.

Very often the structure can not be described by a single dimension number, rather, the dimension number changes from one area into another – these systems are called multi-fractals [28] – an example is available by returning to the length of coastlines problem where the dimension number varies from coast to coast.

Fractal properties can be found in many physical structures, like geographical (length of coastlines, shape of mountain ranges, river deltas, sand dunes), biological (trees, cauliflowers, blood vessels) [29], distribution of minerals in the ground and percolation phenomena [5], distribution of galaxies in the universe [30], distribution of dark matter [31], weather patterns [14, 15, 32], turbulence [8, 9, 33, 34] and mixing in turbulent flow [10]. Another area where fractality can be found are chaotic non-linear systems – fractal structures can be created by systems of differential equations. Signals that are self-affine can be found in many places (like the flow rate of the river Nile [16]) and are often called  $1/f$ -like noises. Even stock market indexes are found to be multi-fractal [35, 36]. We investigate self-similar random processes in the next section in more detail.

## 2.1 SELF-SIMILAR PROCESSES

In this section we proceed to give a more strict definition of self-similarity, its delta variance, the fractional Brownian motion and the power spectral connection.

We denote by  $X(t)$  a random process (also called random function)  $\{X_t\}_{t \in \mathbb{R}}$ , where  $X_t$  are real valued random variables related by some joint distribution

functions. We call higher-dimensional real valued random processes  $\{X_t\}_{t \in \mathbb{R}^n}$  random surfaces or random potentials.

We write  $X(t) \simeq Y(t)$  if the two random processes  $X(t)$  and  $Y(t)$  have the same finite joint distribution functions. We say that a random process  $X(t)$  is self-similar if for any  $|a| > 0$  there exists  $b > 0$  so that

$$X(t) \simeq bX(at). \quad (2.1.1)$$

If the process  $X(t)$  is non-trivial and satisfies a condition of stochastic continuity (continuity with probability one), the constant  $b$  can be rewritten by introducing an exponent  $H$  as

$$X(t) \simeq |a|^{-H} X(at) \quad (2.1.2)$$

with  $H > 0$  [37]. This is also the usual definition given for self-similar random functions. The function  $X(t)$  is also zero at  $t = 0$  almost surely (a.s. – with probability one) [38]. Aside from non-triviality it also makes sense to further assume that  $\langle |X(1)|^2 \rangle < \infty$ . Here  $\langle \cdot \rangle$  denotes mathematical expectation (for physical systems also known as the ensemble average). Clearly, a non-trivial self-similar process is not stationary.

The parameter  $H$  is known as the scaling exponent, as the Hurst exponent, as the Hölder exponent and sometimes values like  $\alpha = 2H$  are used. In the context of non-trivial self-similar processes, the value  $H$  must be constrained by  $0 < H < 1$  [38, 39] (we get  $X(t) = 0$  a.s. when  $H = 0$  and  $X(t) \propto t$  a.s. in case  $H = 1$ ). If one looks at two consequent increments of the process, then with  $H = 0.5$  the sign of the two increments is completely random. With  $H < 0.5$  the signs tend to be opposite and with  $H > 0.5$  the signs tend to be the same – so  $H$  characterises zero, negative or positive correlation of the increments.

We say that a self-similar random process  $X(t)$  has stationary increments if for any given  $t_0$  we have

$$X(t_0 + \Delta t) - X(t_0) \simeq X(\Delta t). \quad (2.1.3)$$

Many physical random processes have stationary increments – how much the value of some quantity statistically changes in a given interval does not depend on the value of the time. A natural example of this kind of self-similar process would be that of the Brownian motion  $B(t)$  of a particle due to thermal agitation. Approximated as a Gaussian process, the variance of relative Brownian motion (also known as Brownian noise) is given as

$$\langle [B(t_2) - B(t_1)]^2 \rangle = 2D_0 |t_2 - t_1|, \quad (2.1.4)$$

where  $D_0$  is the diffusion coefficient [19, p. 988].

We say that a process has self-similar increments when

$$X(t + \Delta t) - X(t) \simeq a^{-H} [X(t + a\Delta t) - X(t)] \quad (2.1.5)$$

and if  $X(t) = 0$  a.s. then the process is self-similar satisfying (2.1.2) [40].

We can derive the covariance of a mean zero self-similar process with stationary increments:

$$\langle X(t) X(s) \rangle = \frac{1}{2} \left\{ |t|^{2H} + |s|^{2H} - |t - s|^{2H} \right\} \langle |X(1)|^2 \rangle. \quad (2.1.6)$$

A random process with stationary increments can be described by another quantity – its delta variance  $\Delta X(\Delta t)$ :

$$\Delta X(\Delta t) \equiv \left\langle [X(t + \Delta t) - X(t)]^2 \right\rangle. \quad (2.1.7)$$

For processes with stationary increments and constant mean  $\Delta X(\Delta t)$  is equal to the variogram of the process:

$$2\gamma(s, t) = \Delta X(s - t). \quad (2.1.8)$$

For a self-similar process with stationary increments we consequently get

$$\Delta X(\Delta t) = |\Delta t|^{2H} \langle |X(1)|^2 \rangle \quad (2.1.9)$$

and

$$\langle X(t) X(s) \rangle = \frac{1}{2} [\Delta X(t) + \Delta X(s) - \Delta X(t - s)]. \quad (2.1.10)$$

Qualitatively, the delta variance describes how much the function should typically change given distance. It can also be interpreted as the squared height of the characteristic features of the given length. If we interpret the random process as a sum of hills (or valleys) on top of bigger hills on top of even bigger hills etc, then the height of the hill (or valley)  $h$  should be a function of the length of the hill  $\lambda$  as  $h \sim \lambda^H$ .

A Gaussian process is defined by its covariance function and mean – hence a mean zero Gaussian process with stationary increments is completely defined by the delta variance function. A Gaussian process that follows (2.1.9) is known as fractional Brownian motion. It is self-similar and with stationary increments. Comparing equations (2.1.4) and (2.1.9) it is easy to see that the regular Brownian motion is fractional Brownian motion with  $H = 0.5$  [39]. Equivalently, fractional

Brownian motion  $B_H(t)$  can also be defined through a Weyl integral over the Brownian noise  $B(s)$  [40]:

$$B_H(t) = \frac{1}{\Gamma(H + \frac{1}{2})} \left\{ \int_{-\infty}^0 \left[ (t-s)^{H-1/2} - (-s)^{H-1/2} \right] dB(s) + \int_0^t (t-s)^{H-1/2} dB(s) \right\}. \quad (2.1.11)$$

Fractional Brownian motion is extensively used as a model for self-similar processes and fractal surfaces.

Fractional Brownian motion curve  $\{t, B_H(t)\}$  is an affine fractal, with the fractal dimension (both box and Hausdorff) given as

$$d_f = d - H, \quad (2.1.12)$$

where  $d$  is the dimension of the motion ( $d = 2$  for a curve) [41]. Self-similar functions and surfaces are often called self-affine. Self-affine random surfaces, in the context of physical systems with a limited scaling range, are also called rough surfaces.

In terms of delta-variance we define fractional Brownian surfaces as Gaussian random surfaces having isotropic delta variance

$$\Delta X(\Delta \mathbf{r}) \propto |\Delta \mathbf{r}|^{2H}. \quad (2.1.13)$$

It is also possible to define fractional Brownian surfaces in a different fashion as an integral of a surface of fractional Brownian noise [40, 42]. This model however does not have stationary increments and so is less useful at modelling physical systems.

Fractional Brownian motion processes were applied for the Monte-Carlo calculations in [P3].

## 2.2 THE SPECTRAL CONNECTION

We now look at spectral aspects of self-similar processes. From [43] the Fourier transform of a function  $f(t)$  is

$$\hat{f}(\omega) \equiv \mathcal{F}[f](\omega) = \int_{-\infty}^{\infty} f(t) e^{-it\omega} dt \quad (2.2.1)$$

and the inverse transform of  $\hat{f}(\omega)$  is

$$\mathcal{F}^{-1}[\hat{f}](t) = \frac{1}{2\pi} \int_{-\infty}^{\infty} \hat{f}(\omega) e^{i\omega t} d\omega. \quad (2.2.2)$$

This integral diverges for fractional Brownian motion as it is not stationary. However, it is possible to work with a truncated subsection of the function

$$f_T(t) = \begin{cases} f(t), & |t| < T, \\ 0, & |t| \geq T. \end{cases} \quad (2.2.3)$$

A Fourier transform exists for the truncated function and we can define the power spectrum of a random process  $X(t)$  as

$$S[X](\omega) = \lim_{T \rightarrow \infty} \left\langle \frac{1}{2T} |\mathcal{F}[X_T](\omega)|^2 \right\rangle, \quad (2.2.4)$$

where  $X_T$  are  $T$ -truncated instances of  $X(t)$ . It turns out that this converges for the fractional Brownian motion as  $T \rightarrow \infty$  [44]. Further, suppose that

$$S[X](\omega) = c\omega^{-2H-1} \quad (2.2.5)$$

with  $0 < H < 1$ . It can be shown ([21, p. 169-173] and [43, p. 206-215]) that  $X(t)$  then has a power law delta variance  $\Delta X(\tau) = C|\tau|^{2H}$ , where the relation between constants  $c$  and  $C$  is given as

$$c = -\frac{\pi C}{2 \sin \frac{\pi(2H+1)}{2} \Gamma(-2H)}. \quad (2.2.6)$$

The converse has also been shown in [44] – fractional Brownian motion has power law power spectrum defined by (2.2.5).

For the isotropic case the power law power spectrum can also be extended into higher-dimensional random potentials:

$$S[X](\omega) \propto |\omega|^{-2H-d}, \quad (2.2.7)$$

where  $d$  is the dimension of the surface  $X$ .

Another interesting property is that the derivative of a random function  $X(t)$  with power law power spectrum  $S[X] = c\omega^{-2H-1}$  has a power law power spectrum  $S[X'] = c\omega^{-2H+1}$ . This is easy to see as the Fourier transform of a derivative is [45]

$$\mathcal{F}[f'] = i\omega \mathcal{F}[f] \quad (2.2.8)$$

and so the power spectrum transforms as

$$S[X'](\omega) = \lim_{T \rightarrow \infty} \left\langle \frac{1}{2T} |i\omega \mathcal{F}[X_T](\omega)|^2 \right\rangle = c\omega^{-2H+1}.$$

This all of course assumes that the function has a derivative (which is hard to define for self-similar processes). Each derivation increases the exponent by 2. Conversely, integration of a random function with power law power spectrum results with the exponent being decreased by 2. This idea is visited later in section 3.3 for generation of random processes for Monte-Carlo simulations – instead of generating the process itself it turns out to be easier to generate the difference function which can be integrated to yield the desired output.

Noises with power law power spectrum are also known as 1/f-like noises, that is they follow a power spectrum  $S[X](f) \propto 1/f^\gamma$ . These noises can be found in many areas [28].

Power law power spectrum can also be found in turbulence. We have the Kolmogorov energy spectrum ( $\gamma = 5/3$ ,  $H = 1/3$ ), weak-turbulent surface gravity waves ( $\gamma = 7/2$ ,  $H = 5/4$ , [8, 9, 46]) and weak-turbulent surface capillary waves ( $\gamma = 19/4$ ,  $H = 15/8$ , [33, 47, 48]). It is reasonable to conclude that the random potentials and surfaces caused by turbulence have fractal properties.

For a Gaussian self-similar processes with power law delta-variance the exponent  $H$  within (2.2.5) is constrained between  $0 < H < 1$ , only in this parameter range do they coincide. Equation (2.2.5) inherently has no problem with values of  $H$  that are outside this range. An example of such a random process is the increment process of fractional Brownian motion (where  $H < 0$ ). So the class of processes with power law power spectrum is wider. Functions with  $H > 1$  on the other hand are almost trivial, they are asymptotically monotonous. Self-similar processes at parameters  $H = 0$  and  $H = 1$  are defined as being almost surely trivial, while by the spectral definition they are not.

Physical systems are finite. The definition of a self-similar process as a model assumes infinite scaling. Suppose we have a Gaussian random process with power law power spectrum only within a given range  $(\omega_m, \omega_0)$ :

$$S[X](\omega) \propto \omega^{-2H-1} \quad \omega_m < \omega < \omega_0 \quad (2.2.9)$$

and outside this range the energy falls off quickly. With  $\lambda_0 \equiv \omega_0^{-1}$  and  $\lambda_m \equiv \omega_m^{-1}$ , we conjecture that the delta variance is also a power law within a range of scales, given by

$$\Delta X(\lambda) \propto |\lambda|^{2H} \quad \lambda_0 \ll \lambda \ll \lambda_m, \quad 0 < H < 1. \quad (2.2.10)$$

This relation has been shown for the Fourier series expansion (and its power function) of a periodic random function [19, p. 986]. As the Fourier transform can be defined through the limit of the Fourier series the relation should apply here.

The power law power spectrum with negative  $H$  is connected to correlated percolation, as described in section 2.5. The spectral view is also used to motivate a simulation method in section 3.5.

### 2.3 SELF-AFFINE FRACTALS AND FRACTAL DYNAMICS

Fractals are not necessarily isotropic – that is they may scale at different rates in different directions. These fractals are called self-affine [49, 50]. The fractional Brownian motion curve or surface  $\{\mathbf{x}, B_H(\mathbf{x})\}$  is a self-affine fractal. It is characterised by the delta-variance, indicating how the height of a section of the curve  $|B_H(\mathbf{x}_2) - B_H(\mathbf{x}_1)|$  typically scales compared to the length  $|\mathbf{x}_2 - \mathbf{x}_1|$ : we have

$$|B_H(\mathbf{x}_2) - B_H(\mathbf{x}_1)| \sim |\mathbf{x}_2 - \mathbf{x}_1|^H \quad 0 < H < 1. \quad (2.3.1)$$

A useful model to study self-affine fractals is the family of self-affine Sierpiński carpets [25, 26, 49, 51]. For the two-dimensional case, these fractals are composed of self-similar elements where a given element's width and height  $a, b$  are related by an exponent  $H$  as  $a \sim b^H$ . The role of the parameter  $H$  is here the same as in the case of the fractal curve of fractional Brownian motion – it describes how the self-similar elements of the fractal scale in different dimensions. Self-affine Sierpiński carpets are used in [P3].

The physical world is often not static. This also applies to fractals. For example, the surface profile of water due to weak-turbulent gravity waves is a function of time. The isolines of the vector potential of two-dimensional turbulent flow change in time. Here, fractality extends into the time dimension – we can look at these phenomena as self-affine spatial-temporal fractals.

Another dynamical aspect can be found in the moving intersections of fractal structures. An example of this would be a river flow – it can be interpreted as an integral of the intersection of rainfall with the river basin (both of which are fractal structures).

Studying these moving intersections of fractal sets was the subject of [P3]. The author's original contribution to the knowledge of physics is the discovery that the measure of the intersections of moving fractal sets is itself a fractal function. We restate this here as follows.

Suppose that we have two sets of points  $F_1$  and  $F_2$ , with either only  $F_1$  or both  $F_1$  and  $F_2$  being fractal, with corresponding fractal dimensions  $D_1$  and  $D_2$ . We

also assume that at least one of the sets is finite, that is it is contained in some ball of radius  $r$ . We may move the set  $F_1$  in some direction  $\hat{n}$ , so that

$$F_1(t) = \{\mathbf{x} + t\hat{n} \mid \mathbf{x} \in F_1\}. \quad (2.3.2)$$

The fractal dimension  $D$  of the intersection  $F_1(t) \cap F_2$ , given that the two sets are statistically independent, is given by equation (2.0.6). The set  $F_2$ , if it is fractal, must have isotropic scaling in all directions. The set  $F_1$  may be self-affine in the direction  $\hat{n}$  with the affine behaviour described by the parameter  $H$  (or  $H = 1$  for a self-similar fractal). In such a case the measure of the intersection  $\mathcal{M}[F_1(t) \cap F_2](t)$  is itself a self-affine function, with its scaling exponent  $h$  given as

$$h = \frac{D}{2H}. \quad (2.3.3)$$

This self-affine scaling is limited by the scaling ranges of the intersecting fractals. Once the movement distance is above the scaling length of a fractal, its fractal dimension is reduced to that of a point or for self-affine two-dimensional fractals, first that of a line. The result presented here was extensively tested by the author using Monte-Carlo calculations.

The derivation of the relation in [P3] is not mathematically rigorous, however, it is supported by the Monte-Carlo simulations – various intersections of fractal structures were tested: by intersecting percolation clusters, self-similar and self-affine Sierpiński carpets, fractional Brownian motion curves; intersections were tested between two fractals structures and also by basic geometric shapes (lines, balls) with a fractal structure.

The author's derivation in [P3] was motivated, as a generalisation for all fractals, by the derivation by supervisor Jaan Kalda for the specific case of intersecting a self-affine function with a moving line. The analytical derivation was done for the simplified case of self-similar fractals.

One of the unanswered questions in [P3] is what happens when the fractals have unisotropic scaling in directions perpendicular to that of movement, or if both sets are self-affine in the direction of movement.

Another interesting aspect to further study would be what happens when the fractal dimension of the intersection is negative. This should result in negative values of  $h$ .

Aside from giving the analytical relation, this result gives descriptive insight into the processes of the physical world. The flow rate of the river Nile, famously studied by Harold Edwin Hurst [16], can be interpreted as an integral quantity of the fractal structure of precipitation over its drainage basin, and as confirmed by the analytical relation we have found, is self-affine. Similarly, the stock market

index indicates the integral output of the economy. Naturally, these phenomena are more complicated in detail but the author believes that their fundamental quality can be described by this result.

## 2.4 PERCOLATION AND CRITICAL PHENOMENA

Percolation refers to the movement and filtering of fluids and gases through porous materials. In the physical world the most obvious examples are the filtering and movement of ground water and pumping of mineral oil or natural gas from porous rock deposits.

Percolation theory studies the properties of these materials through various models, many of which are constructed the following way: we place finite geometric objects (points, line segments, balls, etc) into either a lattice (which can be regular or random) or continuous space. We say that two objects are connected if the distance between them is less than some  $\lambda_0$ . As objects connect together, they form clusters of various shapes. A cluster is said to be infinite if it connects from one end of the lattice to the other. We can then say that the material becomes conductive. In case the placement of objects into the model lattice is random, the emergence of the infinite cluster depends on the lattice site occupation probability  $p$  and one can find the lowest site occupation probability value  $p_c$  where the infinite cluster appears almost surely (in the limit of the lattice size  $a \rightarrow \infty$ ). The value of the  $p_c$ , called the percolation threshold, depends on the dimensionality and type of the lattice.

Near the percolation threshold  $p_c$ , interesting phenomena starts to happen. For one, the formed clusters are fractal and their scaling can be characterised by a fractal dimension. This threshold is a critical point – it causes a second-order phase transition from the material being non-conductive into conductive. Aside from the power law scaling of the cluster mass, many properties of the model show scaling behaviour proportional (in the main singular component, in the limit of lattice size  $L \rightarrow \infty$  and when  $|p - p_c| \ll 1$ ) to the value  $|p - p_c|^{[\sim]}$ , where exponents  $[\sim]$  (usually denoted by the Greek alphabet  $\alpha, \beta, \dots$ ) are called critical exponents. Examples of these include the probability of a lattice site belonging to the infinite cluster

$$P_\infty(p) \propto |p - p_c|^\beta \theta(p - p_c) \quad (2.4.1)$$

or the correlation length

$$\xi(p) \propto |p - p_c|^{-\nu}, \quad (2.4.2)$$

which characterises the size of the cluster distribution – it indicates the maximum size of clusters that can be found.

The remarkable thing is that while the value of  $p_c$  depends on the lattice type, there is numerical and experimental evidence that the fractal scaling and critical exponents only depend on the dimension of the percolation lattice. This is called universality of the scaling exponents. Various critical phenomena, from ferromagnetic transition through the Curie temperature to the conductivity of porous rocks can be placed into universality classes where seemingly unconnected physical systems display the same mathematical scaling laws (with values of the exponents depending on the class).

Aside from percolation, there are other discrete lattice phase transition models. These include the Ising model and the  $q$ -state Potts model. The percolation problem corresponds to a limit of the Potts model for  $q \rightarrow 1$  [52].

An overview of the percolation theory and contemporary problems can be found in [19, 53–55].

## 2.5 CORRELATED PERCOLATION

In the simplest probability model, the lattice sites are occupied independently with a given probability  $p$ . This is called uncorrelated percolation. In case the model contains long-range correlations in the occupation of lattice sites, we start to speak of correlated percolation and the scaling and critical exponents start to change. In physical materials these distortions are usually in the form of defects and their effects are subject to active research [56].

As per universality small changes in the lattice structure should not affect the scaling exponents. It can be shown that small correlations which decay at sufficient speed (against the characteristic cluster size  $\xi$ ) do not affect the behaviour of the system [57]. This is called the Harris criterion.

Suppose that each lattice site has the value  $\theta_i \in \{0, 1\}$ , where 0 denotes unoccupied and 1 denotes occupied. The ensemble average  $\langle \theta_i \rangle_i$  is then the global occupation probability  $p$ . Assuming that the lattice is stationary, we describe the occupation correlation function as

$$c_\theta(\mathbf{x}_i - \mathbf{x}_j) = \langle \theta_i \theta_j \rangle - p^2. \quad (2.5.1)$$

Alternatively, we can denote the occupation probability  $p_i$  of a lattice site as a random number (with  $p = \langle p_i \rangle_i$ ), with correlation function given as

$$c_p(\mathbf{x}_i - \mathbf{x}_j) = \langle p_i p_j \rangle - p^2; \quad (2.5.2)$$

and calculate the occupation site values  $\theta_i$  as

$$\theta_i = \theta(p_i - r), \quad (2.5.3)$$

where  $r$  is a random variable uniformly distributed in  $[0, 1]$  and  $\theta(x)$  is the Heaviside step function. One can show that  $c_\theta(\rho) \equiv c_p(\rho) \equiv c(\rho)$ . While not sufficient to describe all statistical properties, it is believed that the two-point correlation function  $c(\rho)$  contains enough information to determine the critical exponents [19].

From now on we define correlated percolation as percolation where the correlation function follows the algebraic relation

$$c(\rho) \propto |\rho|^{2H}, \quad H < 0. \quad (2.5.4)$$

Site occupation probability  $p_i$  can be described by a continuous random potential  $X$ , where the value of  $p_i$  is taken at coordinate  $x_i$ :

$$p_i = \theta(X(x_i) - r). \quad (2.5.5)$$

It can be shown [19, p. 986] that in case we have an isotropic and stationary mean zero Gaussian random potential with power-law power spectrum as per equation (2.2.9), the correlation function is also a power law, given by

$$c(\rho) \propto \rho^{2H}, \quad \lambda_i \ll \rho \ll \lambda_m, \quad H < 0. \quad (2.5.6)$$

The Harris criterion can be used [19, p. 979] to derive the value of  $H$  where the model still belongs to the universality class of uncorrelated percolation – it is  $H < -1/\nu$  where  $\nu$  is the exponent in equation (2.4.2). For values of  $-1/\nu < H < 0$ , the scaling exponents are functions of  $H$  and we consider this to be the class of correlated percolation. In case of two-dimensional percolation it means that for  $H < -3/4$  the correlations do not affect the critical exponents – in such a case the model belongs to the universality class of uncorrelated percolation. Note that the derivation of the Harris criterion is not mathematically rigorous, while it is supported by numeric evidence.

Equation (2.5.5) allows us to map a random potential into percolation model. Given that mountain ranges are self-affine fractals, one can look at lakes or coastlines as isosets of level water, hence coastlines can be modelled as the edges of a percolation cluster.

As another application of the percolation model, for incompressible turbulent flow, the velocity field can be defined as a curl of the scalar vector potential

$$\mathbf{v}(\mathbf{r}, t) = \nabla \times \Psi(\mathbf{r}, t); \quad (2.5.7)$$

one can further limit the model into a two-dimensional time-independent flow as  $\Psi(x, y, t) = \psi(x, y) \hat{z}$  – here one can study diffusion as movement of tracers along the isolines of the vector potential  $\psi(x, y)$  [10].

For positive values of  $0 < H < 1$  we get an infinite cluster at any probability. While there is no longer a phase transition, the fractality of the clusters remains and their scaling exponents can still be calculated.

## 2.6 SCALING OF TWO-DIMENSIONAL CORRELATED PERCOLATION CLUSTERS

While the percolation cluster is a fractal, other fractal structures can be derived from it: the hull and the unscreened perimeter (see [P1, fig. 4]).

The hull of a percolation cluster is formed by the outside edges of the cluster. This quantity is of importance in the investigation of turbulent diffusion [10]. Its value for the case of two-dimensional uncorrelated percolation is  $d_h = 7/4$  [58].

The unscreened perimeter excludes lattice nodes from the hull that can not be accessed by a ball that is slightly larger than the lattice site size. Its value for the two-dimensional uncorrelated percolation is  $d_p = 4/3$  [59, 60].

The subject of [P1], and the author's original contribution to the knowledge of physics was the numeric calculation of these exponents  $d_h = d_h(H)$  and  $d_p = d_p(H)$  for correlated percolation and clusters formed from self-similar surfaces (rough surfaces) depending on the parameter  $-3/4 < H < 1$  (see [P1, fig. 6]). This calculation was done using Monte-Carlo methods. The results can be seen in [P1, fig. 13].

An overview of previous results can be found in [19, 61]. It is known exactly that  $d_h(0) = 1.5$  [62, 63]. This was confirmed by the calculations.

The calculations ran into convergence problems around  $H = -3/4$  and  $H = 1$  for the hull and the unscreened perimeter, and around  $H = 0$  for the unscreened perimeter. The reasons for the lack of convergence of the unscreened perimeter at  $H = 0$  is without a good answer. The bad convergence at the edges of the theoretical scaling range is most likely caused by the distortions in the random potential used to construct the percolation clusters due to the simulation method and the finiteness of the simulation lattice.

The behaviour of the scaling exponents can be approximated by a stepwise linear function of  $H$ . However, the results of the Monte-Carlo calculations show

a clear divergence from the linear behaviour. This certainly warrants further study. This was previously also observed in [64].

---

## ON SIMULATION OF RANDOM PROCESSES

---

**F**OR MONTE-CARLO INVESTIGATION of statistical properties of self-similar processes one has to generate a vast number of the realisations of the given process with the specified properties, measure them each separately, and then in the end aggregate the result. Generation of self-similar processes is hard due to long-range correlations. Various methods have been developed. Some generate the exact process as specified by mathematical definition, some generate random processes that maintain a desired property like the power law delta variance, some exploit the idea of self-similarity and division of scales in a direct fashion. Aside from accuracy, one also has to consider computational costs – some algorithms are much faster than others. Creation and optimisation of the software for simulations is an essential component of research.

### 3.1 RANDOM NUMBER GENERATION

Monte-Carlo calculations are used to determine the value of some quantity through stochastic sampling of a search space. When determining an expectation of a value whose distribution has a long tail, many samples are necessary to reduce the variance and error bars. Further, the samples have to be truly random (or random enough) so that correlations between samples do not start to compromise the result. There are many algorithms that generate pseudo-random numbers on computers but one has to choose wisely between performance and randomness. A good algorithm to generate random bit sequences allows one to get random numbers of uniform distribution. For the generation of Gaussian random processes and potentials one needs to generate random independent values of normal distribution – these can be calculated from values of uniform distribution.

The author used the Mersenne Twister random number generator by Makoto Matsumoto and Takuji Nishimura [65] – known as the MT19937. The author also tested the ranlux generator [66] which has theoretically proven properties in terms of randomness and long term correlations but found no discernible

difference (aside from speed) when calculating the fractal dimension of the hull of a percolation cluster. A much weaker algorithm (standard C rand) was also tested and produced a clearly incorrect result at larger grid sizes – correlations in the random number sequence started to affect the result. For [P3] and subsequent work the author developed a random process generation software library<sup>1</sup>. Here, a more efficient variation of the Mersenne Twister was used – SFMT (SIMD oriented Fast Mersenne Twister) [67]. This generator makes use of the vectorised calculation units present in modern x86 family processors.

Generation of normally distributed independent random numbers can be done by the use of the Marsaglia polar method [68] which generates two independent normally distributed values  $x, y$  from two uniform random values  $u_1, u_2$ :

$$x = \sqrt{-2 \ln u_1} \cos 2\pi u_2, \quad y = \sqrt{-2 \ln u_1} \sin 2\pi u_2 \quad \text{with} \quad 0 < u_1^2 + u_2^2 < 1. \quad (3.1.1)$$

Unfortunately, the implementation in the GNU Scientific Library – GSL [69] discards the second value and so almost halves the performance. Modern implementation in the c++11 standard library contain reasonable implementations of both the MT19937 and the Marsaglia polar method. However, one can get much higher generation speeds by the use of the Ziggurat algorithm [70]. A variation of this was implemented for the random process generation library. This is a rejection sampling method where the area under the probability distribution curve is divided into horizontal slices of equal area but only on the positive side of the distribution. One can select a slice with uniform distribution. Next, each slice is divided into two – a rectangular area and the area by the curve. Again, uniform random sampling can be used to place the generated number – 98% of them fall into the rectangular area. Here, separate bits from a generated 64-bit random bit sequence can be used for selecting the slice and the first rejection sampling double precision coordinate. Outside the rectangular area a second random number is generated which is tested against the probability distribution function in a standard rejection sampling fashion. If the number falls out of the probability curve, a new number is generated and the test on the horizontal slice is repeated. The sign of the resulting value can be selected by a random bit as normal distribution is symmetric. The tail of the normal distribution has to be handled separately, see [70] for more details.

The speed of the Ziggurat based normal distribution sampling is impressive – over four times the speed of the GSL and three times over the speed of the c++11 standard library.

---

<sup>1</sup> libfbm – <http://mare.ee/indrek/libfbm/>

Aside from vertical scaling on a single CPU core, Monte-Carlo calculations can also be scaled horizontally spreading them over a cluster of machines and CPU cores. Most of the calculations can be done completely independently and only the results have to be aggregated separately. For [P1], a computation cluster at CENS<sup>2</sup> was used. In the modern world cloud based computer resources could be used instead – here computer processing power can be bought quickly, conveniently and with huge capacity.

### 3.2 STATIONARY GAUSSIAN RANDOM PROCESSES

Gaussian random processes can be described by only two functions – the expected value of each coordinate in the process (usually taken as zero) and the two-point covariance function. We are interested in the generation of fractional Brownian motion (one-dimensional) and also fractional Brownian surfaces.

We say that a Gaussian process is stationary and isotropic when the covariance function between the two points does not depend on the coordinates of the points but rather only on the distance between the points, so that

$$\text{Cov}(Z(\mathbf{x}), Z(\mathbf{y})) \equiv \rho(|\mathbf{x} - \mathbf{y}|), \quad (3.2.1)$$

where  $\rho$  is the covariance function. An isotropic process looks the same in each direction. We note here that the fractional Brownian motion as defined in section 2.1 is not stationary, while it is isotropic.

The most direct way to generate processes of multivariate normal distribution is to use Cholesky decomposition on the covariance matrix, that is use the decomposition

$$\Sigma = AA^T. \quad (3.2.2)$$

The covariance matrix is positive semi-definite by definition so such a decomposition must exist. And given a vector of independent normally distributed values  $\mathbf{z} = (z_1, \dots, z_N)^T$ , an instance of the field with the given covariance matrix  $\Sigma$  and mean  $\mu$  simply follows from

$$Z = \mu + Az. \quad (3.2.3)$$

While this method is straightforward and exact, taking the Cholesky decomposition of a very large matrix is impractical. A  $1000 \times 1000$  two-dimensional random process would yield a million by million ( $N = 1000000$ )

---

<sup>2</sup> Centre for Nonlinear Studies at Tallinn University of Technology

covariance matrix. Also, for computations this method requires  $(N + 1) \cdot N/2$  multiplications and additions.

A more efficient generation method is described in [71, 72] to generate stationary Gaussian processes. As said, the fractional Brownian motion is not stationary. However, with a few tricks we can overcome this deficiency.

For a one-dimensional isotropic and stationary Gaussian process the covariance matrix  $\Sigma$  is a Toeplitz matrix (diagonal-constant matrix) and it is completely characterised by its first row  $(c_1, \dots, c_N)$ . A second,  $2N \times 2N$  circular covariance matrix  $S$  is assembled by embedding the covariance matrix  $\Sigma$  within it in a circular fashion, so that the first row of the matrix  $S$  is

$$\mathbf{c} = \left( c_1, \dots, c_N, \frac{c_{N-1} + c_N}{2}, c_{N-1}, \dots, c_1 \right). \quad (3.2.4)$$

The circular matrix  $S$  can be decomposed into

$$S = F\Lambda F^*, \quad \text{where } \Lambda = \text{diag}(F^* \mathbf{c}); \quad (3.2.5)$$

here  $F$  is the discrete Fourier transform in matrix form (with  $F^*$  being the conjugate transpose – the inverse discrete Fourier transform) and  $\Lambda$  is the diagonal matrix of eigenvalues [73]. If the eigenvalues are all non-negative, we can write a decomposition for the matrix  $S$  as  $S = F\Lambda F^* = F\Lambda^{1/2} (F\Lambda^{1/2})^*$ . We recognise here the matrix  $A$  from (3.2.2). Hence, to generate samples of the random process, all we need to do is first calculate the eigenvalues by performing a  $2N$  sized one-dimensional inverse discrete Fourier transform on the vector  $\mathbf{c}$  (using a fast Fourier transform algorithm) and then for each sample take  $2N$  complex values whose components are independent normally distributed random values, multiply them correspondingly with the square roots of the eigenvalues and then take the Fourier transform of the number sequence. The result is two independent number sequences – one in the real component and the other in the imaginary component – taking a subsection of length  $N$  yields us a sample of the random process with covariance given by  $\Sigma$ . Alternatively, we could split the number sequence into two subsections of length  $N$ , however, we must keep in mind that these two sequences are not independent from each other.

For higher-dimensional cases a similar arrangement but with a higher-dimensional Fourier transform can be used, see [72] for more details. For fast Fourier transform the free FFTW3 [74] library provides very good performance (with complexity  $O(n \log n)$ ). For optimal performance the lattice size  $2N$  should be kept a power of two.

It was mentioned that for all this the eigenvalues of  $S$  must be non-negative. There is more here – only in such a case is the matrix  $S$  non-negative definite

and so is a covariance matrix. It can easily happen that for the given covariance matrix  $\Sigma$ , the resulting circular matrix  $S$  is not positive semi-definite. In such a case what can be done is to modify the circular vector  $\mathbf{c}$  by adding appropriate elements in the middle to try to make  $S$  positive-definite. This is a rather vague instruction but good results can be achieved on a case by case basis. This approach is further described in [71, 72, 75].

### 3.3 FRACTIONAL BROWNIAN MOTION AND SURFACES

Fractional Brownian motion is not stationary. However, its increment process, called the fractional Gaussian noise

$$X(t) = B_H(t+1) - B_H(t) \quad (3.3.1)$$

is. The covariance function for  $n$ -dimensional fractional Gaussian noise is given as

$$\rho(\mathbf{r}) = \prod_{i=1}^n \frac{1}{2} \left[ |r_i - 1|^{2H} - 2|r_i|^{2H} + |r_i + 1|^{2H} \right], \quad 0 < H < 1, \quad (3.3.2)$$

see [42] for more details. For the one-dimensional case a noise with this covariance can be generated and then integrated – result is a sample of exact fractional Brownian motion. This method was used for generating the reflection surfaces in [P3].

Unfortunately, this approach does not work for higher-dimensional cases – here a slightly different method is applied as described in [75] which produces random Gaussian processes with power law delta variance. First, how do we define fractional Brownian motion in higher dimensions? We seek random processes whose variogram is a power law. To get here, we first need to define a stationary covariance  $\rho(\mathbf{r})$ :

$$\rho(\mathbf{r}) = \begin{cases} c_0 - |\mathbf{r}|^{2H} + c_2 r^2, & 0 \leq |\mathbf{r}| \leq 1; \\ \frac{\beta(R-|\mathbf{r}|)^3}{|\mathbf{r}|}, & 1 \leq |\mathbf{r}| \leq R; \\ 0, & |\mathbf{r}| > R. \end{cases} \quad (3.3.3)$$

Here  $R \geq 1$  and  $c_0, c_2, \beta$  are chosen so that  $\rho$  is twice differentiable and positive (see [75] for more detail). In the range  $1 \leq |\mathbf{r}| \leq R$  the function  $\rho$  takes the role of the elements inserted in the middle of the vector  $\mathbf{c}$  in the previous section to make the circular matrix  $S$  positive semi-definite. The basic idea here is to simulate a

stationary Gaussian process with correlation function  $c_0 - |\mathbf{r}|^{2H} + c_2 r^2$  in a ball of radius 1. At the edges of the ball and the rest of the simulation grid the correlation function is modified to result in a non-negative definite circular matrix  $S$ .

The resulting process within the ball of radius 1 follows delta variance

$$\frac{1}{2} \text{Var}(Z(\mathbf{x}) - Z(\mathbf{y})) = |\mathbf{x} - \mathbf{y}|^{2H} - c_2 |\mathbf{x} - \mathbf{y}|^2. \quad (3.3.4)$$

This is not yet quite what we want. Post-processing is applied to the process to remove the second term in the following way:

$$Z^*(\mathbf{x}) = Z(\mathbf{x}) + \sum_{i=1}^d x_i 2c_2 X_i, \quad (3.3.5)$$

where  $X_i$  are independent normally distributed random values. The resulting function has a power law delta variance:

$$\frac{1}{2} \text{Var}(Z^*(\mathbf{x}) - Z^*(\mathbf{y})) = |\mathbf{x} - \mathbf{y}|^{2H}. \quad (3.3.6)$$

The covariance of this process however is different from the canonical fractional Brownian motion:

$$\text{Cov}(Z^*(\mathbf{x}), Z^*(\mathbf{y})) = c_0 - |\mathbf{x} - \mathbf{y}|^{2H} + c_2 (|\mathbf{x}|^2 + |\mathbf{y}|^2). \quad (3.3.7)$$

### 3.4 DIRECT USE OF FAST FOURIER TRANSFORM

The fast Fourier transform can be directly applied to generate random processes with power law delta variance at  $0 < H < 0.5$ .

Suppose we have an  $N$ -periodic number sequence  $x[k]$  so that  $x[k] = x[k \bmod N]$ . Its discrete Fourier transform is

$$\hat{x}[k] = \mathcal{F}_N \{x\}[k] = \sum_{n=0}^{N-1} x[n] e^{-i2\pi k n / N} \quad (3.4.1)$$

and the inverse transform is

$$x[k] = \mathcal{F}_N^{-1} \{\hat{x}\}[k] = \frac{1}{N} \sum_{\kappa=0}^{N-1} \hat{x}[\kappa] e^{i2\pi k \kappa / N}. \quad (3.4.2)$$

The periodogram of this number sequence is

$$\mathcal{P}_N \{x\} [k] = \frac{1}{N} |\mathcal{F}_N \{x\} [k]|^2 \quad (3.4.3)$$

and we denote the expectation of the periodogram as

$$\mathcal{S}_N \{x\} [k] = \langle \mathcal{P}_N \{x\} [k] \rangle. \quad (3.4.4)$$

The autocovariance of an  $N$ -periodic sequence  $x[k]$  is

$$\bar{r}_N \{x\} [k] = \frac{1}{N} \sum_{n=0}^{N-1} x[n] x[n+k]. \quad (3.4.5)$$

This can be reinterpreted as a circular discrete convolution. With  $x^- [k] = x[-k]$ ,

$$\bar{r}_N \{x\} [k] = \frac{1}{N} (x^- * x) [-k], \quad (3.4.6)$$

In frequency domain a convolution can be represented as multiplication. Also as  $x[k]$  is real we have the symmetry  $\mathcal{F}_N \{x\} [k] = \overline{\mathcal{F}_N \{x\} [-k]}$ , so we get

$$\mathcal{F}_N \{\bar{r}_N \{x\}\} [k] = \frac{1}{N} |\mathcal{F}_N \{x\} [k]|^2 = \mathcal{P}_N \{x\} [k]. \quad (3.4.7)$$

In other words the autocovariance and the periodogram are Fourier transform pairs. The sample delta variance is

$$\bar{\Delta} \{x\} [k] = \frac{1}{N} \sum_{i=0}^{N-1} (x[i] - x[i+k])^2. \quad (3.4.8)$$

This can be tied to the sample autocovariance and the periodogram:

$$\bar{\Delta} \{x\} [k] = 2\bar{r}_N \{x\} [0] - 2\mathcal{F}_N^{-1} \{\mathcal{P}_N \{x\}\} [k] \quad (3.4.9)$$

and conversely the periodogram can be derived from the given sample delta variance:

$$\mathcal{P}_N \{x\} [k] = \mathcal{F}_N \{\bar{r}_N \{x\} [0]\} - \frac{1}{2} \mathcal{F}_N \{\bar{\Delta} \{x\} [k]\} [k]. \quad (3.4.10)$$

Note that  $\bar{r}_N \{x\} [0]$  in this expression is a constant function and so its Fourier transforms only affects the  $k = 0$  component of the periodogram. The ensemble average periodogram is then

$$\mathcal{S}_N \{x\} [k] = \mathcal{F}_N \{\langle \bar{r}_N \{x\} [0] \rangle\} - \frac{1}{2} \mathcal{F}_N \{\langle \bar{\Delta} \{x\} [k] \rangle\} [k]. \quad (3.4.11)$$

We assume that as a random process  $x[n]$  has stationary increments. Then the ensemble averaged sample delta variance is equal to the ensemble delta variance:

$$\langle \bar{\Delta}\{x\}[k] \rangle = \langle (x[k] - x[0])^2 \rangle. \quad (3.4.12)$$

We want this function to be a power law. However, it also has to be symmetric, that is  $\langle \bar{\Delta}\{x\}[k] \rangle = \langle \bar{\Delta}\{x\}[-k] \rangle$ . This is achieved by the following periodic function:

$$\langle \bar{\Delta}\{x\}[k] \rangle = \begin{cases} (k \bmod N)^{2H}, & k \bmod N < \lfloor N/2 \rfloor \\ (N - k \bmod N)^{2H}, & \text{otherwise} \end{cases}. \quad (3.4.13)$$

From the previously derived equations we get

$$S_N\{x\}[\kappa] = \mathcal{F}_N \left\{ \langle \bar{r}_N\{x\}(0) \rangle - \frac{1}{2} \langle \bar{\Delta}\{x\}[k] \rangle \right\} [\kappa]. \quad (3.4.14)$$

We want the resulting function to have zero mean, hence the  $\kappa = 0$  component of the averaged periodogram must be 0 and so we define

$$\mathcal{F}_N\{\langle \bar{r}_N\{x\}(0) \rangle\}[\kappa] = \begin{cases} \mathcal{F}_N\left\{\frac{1}{2} \langle \bar{\Delta}\{x\} \rangle\right\}[0], & \text{for } \kappa=0; \\ 0, & \text{otherwise.} \end{cases} \quad (3.4.15)$$

We conclude that the function  $S_N\{x\}[\kappa]$  can be easily calculated from the given periodic delta variance. There is, however, one more limitation. The power spectrum can not be negative. We have found that the proposed periodic function does produce positive power spectrum for one-dimensional cases in the range  $0 < H \leq 0.5$ . For values above  $H > 0.5$  one has to modify the periodic delta variance function for longer distances – this in effect reduces the length at which the power-law delta variance is true. For the one-dimensional case the author could find functions that follow the power law delta variance at length  $N/4$  for  $H = 0.95$ . Unfortunately, this was done by process of random trial by error – the author is not aware of an analytical solution to this problem. The method described should also be applicable to higher dimensions.

We now know what the expectation of the periodogram must be. If we were to generate the function in Fourier space, then what would the components be? The process we generate is Gaussian with zero mean. Each component of the resulting function is a weighted sum of a finite number of frequency domain components. This can only be if those components themselves are all Gaussian. They should also be with mean zero, complex and we know their average squared

magnitude (the power spectrum  $S_N \{x\}$ ). Also, as the sequence is real, we must have  $\mathcal{F}_N \{x\} [\kappa] = \overline{\mathcal{F}_N \{x\} [-\kappa]}$ . We choose (c.f. [76])

$$\mathcal{F}_N \{x\} [\kappa] = \sqrt{\frac{1}{2} S_N \{x\} [\kappa]} [\mathcal{N}(0, 1) + i\mathcal{N}(0, 1)], \quad (3.4.16)$$

where  $\mathcal{N}(0, 1)$  are independent normally distributed values. What is left is to take an inverse fast Fourier transform of this number sequence to produce two instances of the random process that exactly follows our specified delta variance law up to length  $N/2$ .

What was described here is very similar to what was done in [75] and described in the previous section – we apply the desired property of the random process up to some length, but farther from that we modify the covariance function so that the resulting covariance matrix wholly is positive semi-definite. So the desired property exists within a range of lengths in the generated process and only diverges at greater lengths.

### 3.5 USE OF SPECTRAL SELF-SIMILARITY AND DIVISION OF SCALES

A completely different approach to simulating self-similar noises is to make use of the self-similarity at different scales directly. As per [19], we can divide the random process  $\Psi(x)$  into components where each component represents a specific scaling length  $\lambda$ :

$$\Psi(x) = \sum_{\lambda_i=2^i\lambda_0} \Psi_{\lambda}(x), \quad (3.5.1)$$

where the component  $\Psi_{\lambda}(x)$  is defined by the partial sum

$$\Psi_{\lambda}(x) = \sum_{1/2 < |k|\lambda < 1} \Psi_k e^{ik \cdot x}; \quad (3.5.2)$$

here  $\Psi_k$  are the Fourier series coefficients at wave vector  $k$  of the process  $\Psi(x)$ :

$$\Psi(x) = \sum_k \Psi_k e^{ik \cdot x}. \quad (3.5.3)$$

There are various ways to approximate the components (3.5.2). In [P1] this was done for the two-dimensional case by a function of a grid of overlapping cones where each cone had diameter  $\lambda$  and height  $\lambda^H \mathcal{R}(-1, 1)$ , where  $\mathcal{R}(-1, 1)$  are independent uniform random values in the range  $(-1, 1)$ . The author tried variations of this method – by using random values of normal distribution instead

of uniform, to add multiple generated noises together (to make the generated surface Gaussian), to offset the various layers by random offset, to offset each cone by random but limited offset, to have the characteristic lengths for each layer to be more gradual (so that  $\lambda_i = \alpha^i$ ,  $\alpha < 2$ ). None of these modifications were found to affect the resulting extracted fractal dimensions.

Another advantage of this approximate method is that it allows for values of  $H < 0$  – this is not possible for self-similar noises by definition.

Alternatively, in a different approach to our approximate layers of coned grids, the division of scales is also achieved by the wavelet synthesis. The author made heavy use of wavelets to verify and analyse the scaling exponents of the generated noises in [P3], but did not experiment with noise synthesis with wavelets. More details about wavelets for self-similar processes can be found in [77, 78].

### 3.6 OTHER METHODS AND REFERENCES

Various approximate methods have been used in the past, among them the turning bands [79] and midpoint displacement [80]. In [61] 1+1-dimensional simulation was used for two-dimensional random process – here two-dimensional noise is generated by adding corresponding components of two one-dimensional noises:

$$\Psi(x, y) = \Psi_1(x) + \Psi_2(y). \quad (3.6.1)$$

In [76] “power law noise” is generated directly through Fourier transform. While the resulting noise is certainly random, using a power law periodogram does not capture the properties of self-similar noise, especially as  $H$  starts to approach 1. The method produces somewhat more reasonable approximation at small or negative values of  $H$ .

### 3.7 MAPPING OF A RANDOM POTENTIAL INTO LAND AND SEA

Given a random two-dimensional process  $X(x, y)$ , we can fix the “sea-level” at  $h_0$ , and define a set of points  $\{(x, y) | X(x, y) > h_0\}$  as land and the rest of the points as sea. Due to universality, we can then look at a connected piece of land as a two-dimensional percolation cluster. If the random process follows power law power spectrum with  $-3/4 < H < 0$ , connected clusters of land correspond to correlated percolation clusters. Further, using equation (2.5.5), we can map the random potential into a regular percolation lattice. This was the method used in [P1] to generate percolation clusters for Monte-Carlo calculations – a random

potential was generated as described in the previous sections and it was mapped into a percolation cluster, whose fractal properties were then measured.

---

CALCULATION OF SCALING EXPONENTS

---

**S**UPPOSE WE ARE GIVEN samples of a random processes and we want to determine whether they are self-similar, and in case they are, what is the value of the scaling exponent. And also we are interested in the range of the power law scaling. This problem needed a solution for [P3] where we transformed one random process into another by method of calculating the mass of a moving intersection of a fractal surface with a line or even another fractal structure.

The first idea would be to make direct use of the delta variance relation (2.1.9). This, however, failed miserably. We are dealing with finite sections of fractals, cut out with some algorithm in a quantised lattice. The resulting random processes contain trends and geometric biases which we have difficulty modelling and describing. The power law scaling only happens within a limited range but also its amplitude varies within the context of a sample. All in all, a different approach was needed.

The second idea would be to use the spectral properties, that is equation (2.2.5). A very naive approach is to calculate the periodogram and fit a line through it. This approach was used in the early days of self-affine process research, but even binning the periodogram components to get a saner fit of the line does not yield accurate results. Another question is, whether one can even get an accurate reading from a single finite sample of the random process. While fractional Brownian motion is ergodic [81], one may still need quite a long stretch of it to determine the exponent with high confidence.

If a single periodogram does not work, perhaps we can work with the expectation of the periodogram (3.4.4) – it would be the finite and discrete equivalent of the continuous power spectrum. But is the expectation of the periodogram even a power law, given that the process we measure actually is self-similar? A result in [43] states that the expectation of the periodogram of  $N$  samples from a discrete time process  $x[k]$  with power spectrum  $S\{x\}(\theta)$  is

$$S_N\{x\}[k] = \int_{-\pi}^{\pi} F_N(\theta - 2\pi k/N) S\{x\}(\theta) d\theta, \quad (4.0.1)$$

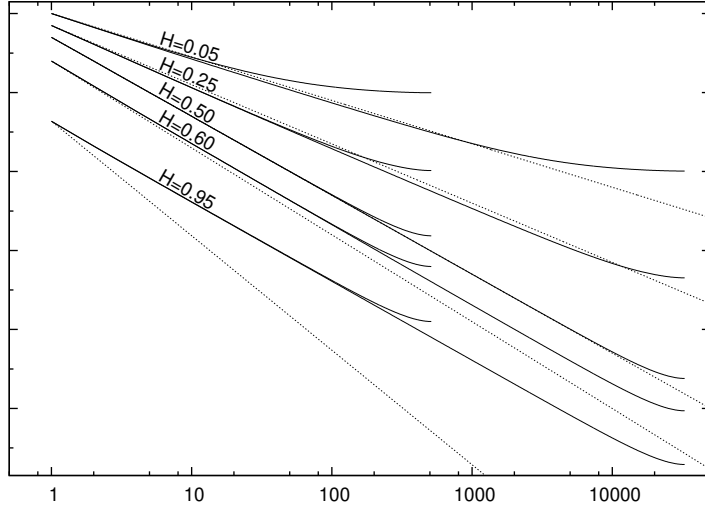


**Figure 1** – Log-log plot of the expectation of the periodogram for fractional Brownian motion at sample counts  $N = 1024$  and  $N = 65536$ . Dotted line is the corresponding power law for the given  $H$ .

where  $F_N$  is the Fejer kernel

$$F_N(\theta) = \frac{1}{2\pi} \cdot \frac{\sin^2(N\theta/2)}{N \sin^2(\theta/2)}. \quad (4.0.2)$$

As can be seen in figure 1 the expectation of the periodogram for a random process with power law power spectrum does not form a straight line with the slope of the line determined by the exponent  $H$  in a log-log plot for larger values of  $H$  (appearing as  $H = 0.5$  for  $H > 0.5$ ). The periodogram just is not a good approximation of the power spectrum. For small or negative values of  $H$  it might give a reasonable approximation. The reason is that the finite Fourier transform assumes that the function is periodic, while with  $H > 0.5$  the random process tends to follow a trend for long stretches. Author also tried modifications of the function (like subtracting a linear function) to “make” it periodic, but these efforts did not yield reasonable results.

When the analysed noises contain distortions, both direct delta-variance and spectral methods fall short. The wavelet method is designed to bypass global trends in the signal and so should produce very good results for this application. Next, we look how it can be used to analyse self-similar noises.

#### 4.1 THE WAVELET METHOD

First, we look at some basic ideas of the wavelet theory. We say that  $f \in L^p(\mathbb{R})$  if

$$\int_{\mathbb{R}} |f(t)|^p dt < +\infty. \quad (4.1.1)$$

Suppose we have some function  $\Psi \in L^1(\mathbb{R}) \cap L^2(\mathbb{R})$ . From this, we create another, parametric function

$$\Psi_{\lambda,\tau}(t) = \frac{1}{\sqrt{\lambda}} \Psi\left(\frac{t-\tau}{\lambda}\right), \quad (4.1.2)$$

where parameter  $\lambda > 0$  scales and parameter  $\tau$  translates the original function. Function  $\Psi$  is called the mother wavelet, and the family of functions  $\Psi_{\lambda,\tau}$  are called the daughter wavelets. Given a function  $f \in L^2(\mathbb{R})$ , the scalar product  $\langle f, \Psi_{\lambda,\tau} \rangle$  characterises the contribution of the daughter wavelet into function  $f$ . We define another function through this scalar product as

$$\mathcal{W}[f](\lambda, \tau) = \langle f, \Psi_{\lambda,\tau} \rangle = \int_{\mathbb{R}} f(t) \overline{\Psi_{\lambda,\tau}(t)} dt. \quad (4.1.3)$$

Function  $\mathcal{W}[f]$  is called the continuous wavelet transform of function  $f$  using the wavelet  $\Psi$ . The continuous wavelet transform  $\mathcal{W}[f]$  indicates how much the wavelet  $\Psi$  resonates with function  $f$  at the given scale (against the scaled frequencies contained in the wavelet) and position. In case  $\int_{\mathbb{R}} \frac{1}{|\nu|} |\mathcal{F}[\Psi](\nu)|^2 d\nu < \infty$ , an inverse transform also exists:

$$f(t) = \int_0^\infty \int_{\mathbb{R}} \mathcal{W}[f](\lambda, \tau) \Psi_{\lambda,\tau}(t) d\tau \frac{d\lambda}{\lambda^2}. \quad (4.1.4)$$

A plotted visualisation of  $|\mathcal{W}[f](\lambda, \tau)|^2$  (usually, as a coloured map) is known as the scalogram. While the Fourier transform characterises only the frequency distribution of a function, the wavelet transform gives us an idea also about the location where the signal resonates with the wavelet.

It makes sense to choose wavelets that have a compact support (the range of points where  $\Psi$  is nonzero is bound) as it simplifies calculation. Further, some functions work better as wavelets than others, depending on the application – the capacity to isolate the frequency (scale) and location varies from function to function. Examples of the continuous wavelets that are widely used would be the Mexican hat wavelet (also called the Ricker wavelet, with compact support) [82]

and the Shannon wavelet (without compact support) [83]. Wavelets are used for signal analysis, image compression and solving PDE-s (see [84] for an overview).

There also exists a discrete wavelet transform (and corresponding fast wavelet transform) that can be efficiently applied on discrete data series – here we need an orthonormal system of wavelets

$$\Psi_{j,k}(t) = 2^{j/2} \Psi(2^j t - k) \quad j, k \in \mathbb{Z} \quad (4.1.5)$$

so that

$$\langle \Psi_{j,k}, \Psi_{l,m} \rangle = \begin{cases} 1, & \text{when } j = l, k = m \\ 0, & \text{otherwise.} \end{cases} \quad (4.1.6)$$

Finding such wavelets is rather involved and is done through multiresolution analysis. The most famous discrete wavelets are the Daubechies family of wavelets (enumerated based on the number of base coefficients, with D2, D4, D6, ...; where D2 is the Haar wavelet) [84].

Another important property of the DN Daubechies wavelets is that they have been constructed to have  $N/2$  vanishing moments, that is

$$\langle t^m, \Psi \rangle = 0, \quad 0 \leq m \leq N/2. \quad (4.1.7)$$

In such a case the polynomial components of the analysed signal are not represented in the wavelet transform coefficients. For analysing signals this is a very useful property as it excludes trend lines or polynomial distortions in the signal that may be caused by external factors, instrumentation, finiteness of the process or due to simulation lattice geometry in Monte-Carlo calculations.

Next, we follow [78] for applying the wavelet transform to analyse self-similar noises. Given a self-similar random process  $X(t)$  (satisfying equation (2.1.2)) we should have for the wavelet transform a similar relation

$$\mathcal{W}[X(t)](\lambda, \tau) \simeq \mathcal{W}\left[|a|^{-H} X(at)\right](\lambda, \tau). \quad (4.1.8)$$

Substituting  $|a|^{-H} X(at)$  into (4.1.3) yields

$$\mathcal{W}[X](a\lambda, a\tau) \simeq |a|^{H+1/2} \mathcal{W}[X](\lambda, \tau). \quad (4.1.9)$$

Next, we make use of the averaged transform over all the translations with a fixed scale:

$$\mathcal{W}[X](\lambda) \equiv \lim_{T \rightarrow \infty} \frac{1}{2T} \int_{-T}^T \mathcal{W}[X](\lambda, \tau) d\tau. \quad (4.1.10)$$

For an ergodic self-similar process, this is actually the expectation. In case it converges, we should have

$$W[X](a\lambda) = |a|^{H+1/2} W[X](\lambda); \quad (4.1.11)$$

this can only be if

$$W[X](\lambda) \propto \lambda^{H+1/2}. \quad (4.1.12)$$

For the discrete wavelet transform we can simply take the arithmetic mean of the wavelet coefficients at the given scale as estimate of the expectation. For Monte-Carlo simulations one can calculate the average coefficients over many samples, plot them on a log-log graph, and conclude that in any place where the graph is linear the process is self-similar with parameter  $H$  that can be extracted from the slope of the line.

The method outlined was extensively used in [P3] for estimating the scaling exponents of the produced noises and yielded superior results compared to all other tested methods. The author found that the D4 wavelet did not work as well as D6-D12. Author also used the Mexican hat wavelet through numeric integration and found that it also produced acceptable results. The method was also tested on noises with negative  $H$  and was found to work in such a case.

## 4.2 FRACTAL SCALING EXPONENTS AND FINITE SIZE EFFECTS

The previous methods can be applied to self-affine curves and surfaces. We now turn our attention into calculating the scaling exponents of self-similar fractals. In Monte-Carlo calculations this is done by generating fractals, measuring their size (radius or diameter of the smallest ball that contains them) and mass (in a regular lattice, the number of sites occupied), and trying to relate these quantities as per equation (2.0.5). As there can be a lot of variation, millions of instances of fractals must be generated to arrive at a consistent result. Further, one must pick a good method how to fuse and average several measurements together as each may have a different size value.

For the application of calculating the scaling exponents of two-dimensional correlated percolation cluster hull, the following method was used in [P1]: we use quantised lattice sizes ( $\chi \in \{8, 16, 32, \dots, \chi_{\max}\}$ ) and generate a correlated or self-similar random potential as per the parameter  $H$ ; then we set the sea-level so that the centre lattice site is land. We then trace the percolation cluster hull from this site until it reaches the edges of the lattice and measure its length. If the hull makes a loop instead of reaching the edge, we discard the sample and start over. This is repeated millions of times for the given lattice size  $\chi$  and the

average length  $\overline{L(x)}$  is calculated. If the hull is a fractal, the expectation of  $L(x)$  should scale as

$$\langle L(x) \rangle \propto x^{d_h(H)}. \quad (4.2.1)$$

Alternatively, we may use a periodic lattice but only use hulls that penetrate the edge of the lattice. The calculation of the unscreened perimeter can be done in a similar fashion.

We could now plot the data points on a log-log graph, fit a straight line against the points and use its slope as the resulting fractal dimension value. Unfortunately, for lower values of  $x$  the calculated average diverges significantly from the predictions. This is known as the finite size effect – the finite size of the lattices affects the result. We are interested in the exponent in the limit  $x \rightarrow \infty$ . The calculation capacity of modern computers does not allow one to calculate at infinite size as that would require infinite computer memory and CPU capacity.

The finite size effects have the following causes: the lattice fine structure that affects the scaling at finite lengths (discussed in [85–87]), the limited size of the lattice (and how we determine the diameter of the fractal), and errors from the approximation of the statistical model of the lattice occupation. The analytical formulae for the distortions depend on the lattice type and the specifics of the calculation method. It would be nice to have a general method that compensates for these problems.

The author’s contribution to the knowledge of physics involved the testing, verification and publishing of a general method to compensate against the finite size effects in the context of Monte-Carlo calculations [P2]. This method was developed by the author’s supervisor Jaan Kalda and first used in [61]. The method makes a series of constraining assumptions about the measured quantity, but also provides a way to test these assumptions. We outline the gist of the method here.

First, we note that the mass of a fractal can be measured in different ways. Aside from simply counting the number of occupied sites, for the hull, we might count the number of sites that are connected to only one other site. This quantity should also behave according to equation (4.2.1). Samples of these quantities can be found in [P1, fig. 9] and [P2, fig. 2]. In case of Monte-Carlo calculations, where we control all the variables, it is very easy and computationally efficient to calculate these different measurements – they come for free.

Suppose that we find  $m$  different ways to measure the fractal. Next, we assume that these different measurements of the hull length (or the mass of the measured fractal) have the form

$$\langle L_j(x) \rangle = \sum_{k=1}^m A_{jk} x^{\alpha_k} + \Delta_j(x), \quad j = 1 \dots m; \quad (4.2.2)$$

where  $\alpha_k > \alpha_{k+1}$  are the  $m$  main scaling exponents (with  $d_h = \alpha_1$ ) and  $\Delta_j(x)$  represent the remainder of the finite size effects. We further assume, that within the scope of the Monte-Carlo calculations, the values of  $\Delta_j(x)$  are small enough to be statistically insignificant. The coefficients  $A_{jk}$ , for a fixed exponent index  $k$ , are different – the different ways of measuring the fractal structure provide us with further information and data for model fitting.

After calculating all the  $\overline{L_j(x)}$ , we could use some sort of maximum likelihood estimator to calculate the unknown parameters  $A_{jk}$  and  $\alpha_k$ , assuming that  $\Delta_j(x) \approx 0$ . The author tested the Levenberg-Marquardt algorithm [88, p. 801] which does work. However, these methods require a good idea about the initial values of the searched parameters and can easily get stuck in local minima. It is hard to tell if you have the correct result.

The developed method reduces this complicated multi-dimensional search for the best set of parameters into a one-dimensional search on a constructed fitness function, where we test the shape of the fitness function (requiring it to have exactly  $m$  distinct minima) and the fitness of the result by measuring the width of these minima.

The method was applied in [P1] and in general produced very good results. However, as discussed in section 2.6, problems were encountered at some points of the scaling exponents where clearly the form (4.2.2) did not apply.

---

## CONCLUSIONS AND FURTHER WORK

---

**I**N THIS WORK we have studied the statistical topography of self-affine random potentials: properties of two-dimensional correlated percolation clusters by use of Monte-Carlo calculation [P1]; developed a method to efficiently perform Monte-Carlo calculations to determine the scaling exponents of fractals [P2]; and investigated the properties of signals resulting from intersections of moving or evolving fractal sets by deriving an analytical result and testing it numerically [P3].

The inherent randomness of these processes means that the laws we find are statistical, they characterise the average behaviour; we can state where a typical system might evolve to – but are quite limited when working with a single sample.

The happy circumstance of universality means that varied physical systems of disordered media follow the same kind of laws, with variance only in values of parameters. Universality divides into classes; and the task of physicists is to analyse the behaviour for each class and tabulate the values of the parameters. This was the subject of [P1] – finding the scaling exponents of the hull and the unscreened perimeter of percolation clusters for the universality class of two-dimensional correlated percolation and rough surfaces. The results were clear for a range of parameters, confirming previous conjecture and numerical results. However, at specific points of  $H = -3/4$ ,  $H = 1$  for the hull and also at  $H = 0$  for the unscreened perimeter, the calculations failed to converge. The exact reasons for this were left unanswered. Is the convergence inherently slow at these parameters or was it caused by the calculation method or the lattice structure or the inaccuracy of the statistical model used to generate Monte-Carlo samples? We can blame some of the problems to finite size effects, our calculations do simulate a system of limited size. The analytical results are usually taken in the limit of the process scaling range approaching infinity; however, we must recognise that most real physical systems are actually finite. Could we find universal laws for finite scaling?

While the scaling exponents as functions of the parameter  $H$  have been conjectured to be step-wise linear functions, the calculations clearly show a

statistically significant deviation from linear behaviour. It would be interesting to find an analytical relation instead of only relying on numerics.

In [P2] we developed a method to efficiently perform Monte-Carlo calculations. These types of calculations can take a lot of computational resources; the method greatly improves the practicality of Monte-Carlo methods. Also, getting a reliable result requires testing the result against a mathematical model; this is incorporated into the method. The method overcomes a certain type of common finite-size effects encountered in these kind of Monte-Carlo calculations. While very powerful, it still failed in [P1] at certain parameter points. The method is general and one should be able to apply it in varied areas.

Monte-Carlo calculations involve a lot of technical work; in this thesis we have described many of these details including on how to generate samples of random structures corresponding to the assumed statistical model, to analysing fractal signals to determine the scaling parameters.

The work done in [P3] investigated the signals generated by finite intersections of moving fractal sets, or a fractal set intersecting with a primitive geometrical object (a point, a line, a plane, etc.). We found that these signals are self-affine and derived an analytical relation describing their scaling exponent as a function of the fractal dimension of the intersection and the self-affine properties of the intersecting fractals. The derived relation was numerically tested by various types of constructed fractal sets.

Further, this relation was initially motivated by the integral reflection of light from a self-affine fractal surface as a function of reflection angle. It would be interesting to extend this approach and apply the derived relation to the problem of integral reflections from a dynamical surface (for example, due to weak-turbulent gravity waves). This would result in a spatial-temporal fractal structure that has different self-affine scaling in multiple dimensions. For Monte-Carlo calculations to numerically verify any kind of result, one would also need to develop a method to accurately and efficiently simulate these kind of structures.

While the author believes that the derived result is correct, it would be interesting to see a mathematically rigorous proof. The derived relation also allows self-affine behaviour only in the direction of movement, assuming isotropic self-similarity in other directions, and by only one of the structures. A generalisation to treat all cases should be possible.

A moving ball of radius  $r$  intersecting with a fractal structure appears, at movement lengths greater than  $r$ , as a point. The resulting fractal dimension of such intersection is negative. While untested, the derived relation for the scaling exponent of the resulting noise should also work in this case.

Monte-Carlo simulations provide a stable environment to test statistical models and properties, however, a quantitative application of the found relation in the physical world, outside of simulation, would be interesting.

In nature, random fractal structures caused by complex phenomena interact and produce new behaviour. So, the derived relation, while being analytical, also gives descriptive insight into the functioning of nature.



---

## BIBLIOGRAPHY

---

- [1] B. B. Mandelbrot. *The Fractal Geometry of Nature*. Freeman, New York, 1982.
- [2] J. Laskar. Large-scale chaos in the Solar System. *Astronomy and Astrophysics*, 287:L9–L12, 1994.
- [3] W. B. Hayes. Is the outer Solar System chaotic? *Nature Physics*, 3(10):689–691, October 2007.
- [4] S. H. Strogatz. *Nonlinear Dynamics and Chaos*. CRC Press, May 2018.
- [5] P. R. King, S. V. Buldyrev, N. V. Dokholyan, S. Havlin, Y. Lee, G. Paul, H. E. Stanley, and N. Vandesteeg. Predicting oil recovery using percolation theory. *Petroleum Geoscience*, 7(S):S105–S107, March 2001.
- [6] A. Kreyssig, R. Prozorov, C. D. Dewhurst, P. C. Canfield, R. W. McCallum, and A. I. Goldman. Probing Fractal Magnetic Domains on Multiple Length Scales in Nd<sub>2</sub>Fe<sub>14</sub>B. *Physical Review Letters*, 102(4):047204, January 2009.
- [7] A. N. Kolmogorov. The local structure of turbulence in incompressible viscous fluid for very large Reynolds numbers. *Proceedings of the USSR Academy of Sciences*, 30:299–303, 1941.
- [8] A. I. Dyachenko, A. O. Korotkevich, and V. E. Zakharov. Weak turbulence of gravity waves. *Journal of Experimental and Theoretical Physics Letters*, 77(10):546–550, May 2003.
- [9] A. I. Dyachenko, A. O. Korotkevich, and V. E. Zakharov. Weak Turbulent Kolmogorov Spectrum for Surface Gravity Waves. *Physical Review Letters*, 92(13):134501, April 2004.
- [10] M. Isichenko and J. Kalda. Statistical topography, II. Two-dimensional transport of a passive scalar. *Journal of Nonlinear Science*, 1(4):375–396, 1991.
- [11] J. Fossum, H. Bergene, A. Hansen, B. O’Rourke, and G. Manificat. Self-affine crossover length in a layered silicate deposit. *Physical Review E*, 69(3):036108, March 2004.

- [12] B. B. Mandelbrot. How long is the coast of Britain? Statistical self-similarity and fractional dimension. *Science (New York, N.Y.)*, 156(3775):636–8, May 1967.
- [13] G. Dietler and Y.-C. Zhang. Fractal aspects of the Swiss landscape. *Physica A: Statistical Mechanics and its Applications*, 191(1-4):213–219, December 1992.
- [14] S. Lovejoy and B. B. Mandelbrot. Fractal properties of rain, and a fractal model. *Tellus A*, 37A(3):209–232, May 1985.
- [15] S. Lovejoy and D. Schertzer. Multifractals, universality classes and satellite and radar measurements of cloud and rain fields. *Journal of Geophysical Research*, 95(D3):2021, 1990.
- [16] H. E. Hurst. Long Term Storage Capacity of Reservoirs. *Trans. Am. Soc. Civ. Eng.*, 116:770–799, 1951.
- [17] J. M. Ziman. *Models of Disorder: The Theoretical Physics of Homogeneously Disordered Systems*. Cambridge University Press, 1979.
- [18] L. F. Richardson. *General Systems Yearbook*, volume 6 (139). 1961.
- [19] M. B. Isichenko. Percolation, statistical topography, and transport in random media. *Rev. Mod. Phys.*, 64(4):961, 1992.
- [20] J. Feder. *Fractals*. Springer US, Boston, MA, 1988.
- [21] K. Falconer. *Fractal Geometry*. John Wiley & Sons, Ltd, Chichester, UK, September 2003.
- [22] B. B. Mandelbrot. Fractals in physics: Squig clusters, diffusions, fractal measures, and the unicity of fractal dimensionality. *Journal of Statistical Physics*, 34(5-6):895–930, March 1984.
- [23] B. B. Mandelbrot. Negative fractal dimensions and multifractals. *Physica A: Statistical Mechanics and its Applications*, 163(1):306–315, February 1990.
- [24] H. von Koch. Sur une courbe continue sans tangente, obtenue par une construction géométrique élémentaire. *Arkiv för matematik, astronomi och fysik*, 1, 1904.
- [25] W. Sierpiński. Sur une courbe cantorienne qui contient une image biunivoque et continue de toute courbe donnée. *C. R.*, 162:629–632, 1916.
- [26] C. McMullen. The Hausdorff dimension of general Sierpiński carpets. *Nagoya Math. J.*, 96:1–9, 1984.

- [27] Y. Gui and W. Li. A random version of McMullen-Bedford general Sierpiński carpets and its application. *Nonlinearity*, 21(8):1745–1758, August 2008.
- [28] B. B. Mandelbrot. *Multifractals and 1/f Noise*. Springer New York, New York, NY, 1999.
- [29] A. Gamba, D. Ambrosi, A. Coniglio, A. de Candia, S. Di Talia, E. Giraud, G. Serini, L. Preziosi, and F. Bussolino. Percolation, Morphogenesis, and Burgers Dynamics in Blood Vessels Formation. *Physical Review Letters*, 90(11):1–4, March 2003.
- [30] L. Pietronero. The fractal structure of the universe: Correlations of galaxies and clusters and the average mass density. *Physica A: Statistical Mechanics and its Applications*, 144(2-3):257–284, August 1987.
- [31] C. Chacón-Cardona, R. Casas-Miranda, and J. Muñoz-Cuartas. Multi-fractal analysis and lacunarity spectrum of the dark matter haloes in the SDSS-DR7. *Chaos, Solitons & Fractals*, 82:22–33, January 2016.
- [32] R. Ray, M. H. Khondekar, K. Ghosh, and A. K. Bhattacharjee. Scaling and nonlinear behaviour of daily mean temperature time series across India. *Chaos, Solitons & Fractals*, 84:9–14, March 2016.
- [33] A. Pushkarev and V. Zakharov. Turbulence of capillary waves: theory and numerical simulation. *Physica D: Nonlinear Phenomena*, 135(1-2):98–116, January 2000.
- [34] A. S. Lanotte, S. K. Malapaka, and L. Biferale. On the vortex dynamics in fractal Fourier turbulence. *The European Physical Journal E*, 39(4):49, April 2016.
- [35] B. B. Mandelbrot and R. L. Hudson. *The (mis)Behaviour of Markets: A Fractal View of Risk, Ruin and Reward*. Profile Books, 2004.
- [36] M. Lee, J. W. Song, J. H. Park, and W. Chang. Asymmetric multi-fractality in the U.S. stock indices using index-based model of A-MFDFA. *Chaos, Solitons & Fractals*, 97:28–38, April 2017.
- [37] J. Lamperti. Semi-stable stochastic processes. *Transactions of the American Mathematical Society*, 104(1):62–62, January 1962.
- [38] W. Vervaat. Sample Path Properties of Self-Similar Processes with Stationary Increments. *The Annals of Probability*, 13(1):1–27, February 1985.

- [39] P. Embrechts and M. Maejima. An introduction to the theory of self-similar stochastic processes. *International Journal of Modern Physics B*, 14(12n13):1399–1420, May 2000.
- [40] B. B. Mandelbrot and J. W. Van Ness. Fractional Brownian Motions, Fractional Noises and Applications. *SIAM Review*, 10(4):422–437, October 1968.
- [41] S. Orey. Gaussian sample functions and the Hausdorff dimension of level crossings. *Zeitschrift für Wahrscheinlichkeitstheorie und Verwandte Gebiete*, 15(3):249–256, 1970.
- [42] H. Qian, G. M. Raymond, and J. B. Bassingthwaite. On two-dimensional fractional Brownian motion and fractional Brownian random field. *Journal of Physics A: Mathematical and General*, 31(28):L527–L535, July 1998.
- [43] M. B. Priestley. *Spectral analysis and time series*. 1981.
- [44] P. Flandrin. On the spectrum of fractional Brownian motions. *IEEE Transactions on Information Theory*, 35(1):197–199, 1989.
- [45] D. C. Champeney. *A Handbook of Fourier Theorems*. Cambridge University Press, Cambridge, 1987.
- [46] A. O. Korotkevich, A. I. Dyachenko, and V. E. Zakharov. Numerical simulation of surface waves instability on a homogeneous grid. *Physica D: Nonlinear Phenomena*, 321-322:51–66, 2016.
- [47] V. E. Zakharov and N. N. Filonenko. Weak turbulence of capillary waves. *Journal of Applied Mechanics and Technical Physics*, 8(5):37–40, 1971.
- [48] Y. Pan and D. K. P. Yue. Direct Numerical Investigation of Turbulence of Capillary Waves. *Physical Review Letters*, 113(9):094501, August 2014.
- [49] B. B. Mandelbrot. Diagonally self-affine fractal cartoons. Part 3: "anomalous" Hausdorff dimension and multifractal "localization". In *Fractals in Physics: Proceedings of the Sixth Trieste International Symposium on Fractals in Physics*, pages 463–480, Trieste, 1985. Elsevier Science Ltd.
- [50] B. B. Mandelbrot. Self-Affine Fractals and Fractal Dimension. *Physica Scripta*, 32(4):257–260, October 1985.
- [51] T. J. Bedford. *Crinkly curves, Markov partitions and dimension*. Phd, University of Warwick, 1984.

- [52] C. Fortuin and P. Kasteleyn. On the random-cluster model. *Physica*, 57(4):536–564, February 1972.
- [53] D. Stauffer and A. Aharony. *Introduction to Percolation Theory*. Taylor & Francis, London, 1992.
- [54] B. Bollobas and O. Riordan. *Percolation*. Cambridge University Press, Cambridge, 2006.
- [55] N. Araújo, P. Grassberger, B. Kahng, K. Schrenk, and R. Ziff. Recent advances and open challenges in percolation. *The European Physical Journal Special Topics*, 223(11):2307–2321, October 2014.
- [56] J. Zierenberg, N. Fricke, M. Marenz, F. P. Spitzner, V. Blavatska, and W. Janke. Percolation thresholds and fractal dimensions for square and cubic lattices with long-range correlated defects. *Physical Review E*, 96(6):062125, December 2017.
- [57] A. B. Harris. Effect of random defects on the critical behaviour of Ising models. *Journal of Physics C: Solid State Physics*, 7(9):1671–1692, May 1974.
- [58] H. Saleur and B. Duplantier. Exact Determination of the Percolation Hull Exponent in Two Dimensions. *Phys. Rev. Lett.*, 58(22):2325–2328, 1987.
- [59] T. Grossman and A. Aharony. Structure and perimeters of percolation clusters. *Journal of Physics A: Mathematical and General*, 19:L745–L751, 1986.
- [60] T. Grossman and A. Aharony. Accessible external perimeters of percolation clusters. *J. Phys. A: Math Gen*, 20:L1193–L1201, 1987.
- [61] J. Kalda. Statistical topography of rough surfaces: "Oceanic coastlines" as generalizations of percolation clusters. *EPL (Europhysics Letters)*, 84(4):46003 (6pp), 2008.
- [62] J. Kondev and C. L. Henley. Geometrical Exponents of Contour Loops on Random Gaussian Surfaces. *Physical Review Letters*, 74(23):4580–4583, 1995.
- [63] J. Kondev, C. L. Henley, and D. G. Salinas. Nonlinear measures for characterizing rough surface morphologies. *Physical Review E*, 61(1):104–125, 2000.
- [64] J. Kalda. Description of random Gaussian surfaces by a four-vertex model. *Phys. Rev. E*, 64(3):020101(R), 2001.

- [65] M. Matsumoto and T. Nishimura. Mersenne twister: a 623-dimensionally equidistributed uniform pseudo-random number generator. *ACM Transactions on Modeling and Computer Simulation*, 8(1):3–30, January 1998.
- [66] M. Lüscher. A portable high-quality random number generator for lattice field theory simulations. *Computer Physics Communications*, 79(1):100–110, 1994.
- [67] M. Saito and M. Matsumoto. SIMD-Oriented Fast Mersenne Twister: a 128-bit Pseudorandom Number Generator. In *Monte Carlo and Quasi-Monte Carlo Methods 2006*, pages 607–622. Springer Berlin Heidelberg, Berlin, Heidelberg, 2008.
- [68] G. Marsaglia and T. A. Bray. A Convenient Method for Generating Normal Variables. *SIAM Review*, 6(3):260–264, July 1964.
- [69] M. Galassi. *GNU Scientific Library Reference Manual (3rd Ed.)*. 2009.
- [70] G. Marsaglia and W. W. Tsang. The Ziggurat Method for Generating Random Variables. *Journal of Statistical Software*, 5(8):1–7, 2000.
- [71] C. R. Dietrich and G. N. Newsam. Fast and Exact Simulation of Stationary Gaussian Processes through Circulant Embedding of the Covariance Matrix. *SIAM Journal on Scientific Computing*, 18(4):1088–1107, July 1997.
- [72] A. T. A. Wood and G. Chan. Simulation of Stationary Gaussian Processes in  $[0, 1]^d$ . *Journal of Computational and Graphical Statistics*, 3(4):409–432, December 1994.
- [73] G. H. Golub and C. F. Van Loan. *Matrix Computations (Johns Hopkins Studies in the Mathematical Sciences)*. 4th edition, 2012.
- [74] M. Frigo and S. Johnson. The Design and Implementation of FFTW3. *Proceedings of the IEEE*, 93(2):216–231, February 2005.
- [75] M. L. Stein. Fast and Exact Simulation of Fractional Brownian Surfaces. *Journal of Computational and Graphical Statistics*, 11(3):587–599, September 2002.
- [76] J. Timmer and M. König. On generating power law noise. *Astronomy and Astrophysics*, 300:707, 1995.
- [77] C. Heneghan, S. Lowen, and M. Teich. Two-dimensional fractional Brownian motion: wavelet analysis and synthesis. *Proceedings of the IEEE Southwest Symposium on Image Analysis and Interpretation, 1996.*, pages 213–217, 1996.

- [78] I. Simonsen, A. Hansen, and O. Nes. Determination of the Hurst exponent by use of wavelet transforms. *Physical Review E*, 58(3):2779–2787, September 1998.
- [79] Z.-M. Yin. New methods for simulation of fractional Brownian motion. *Journal of computational physics*, 127(1):66–72, 1996.
- [80] M. A. Stoksik, R. Lane, and D. Nguyen. Practical Synthesis of Accurate Fractal Images. *Graphical Models and Image Processing*, 57(3):206–219, May 1995.
- [81] W. Deng and E. Barkai. Ergodic properties of fractional Brownian-Langevin motion. *Physical Review E*, 79(1):011112, January 2009.
- [82] J. W. J. Hosken. Ricker wavelets in their various guises. *First Break*, 6(1):24–33, 1988.
- [83] C. Cattani. Shannon wavelets theory. *Mathematical Problems in Engineering*, 2008.
- [84] I. Daubechies. *Ten Lectures on Wavelets*. Society for Industrial and Applied Mathematics, January 1992.
- [85] R. Ziff. Correction-to-scaling exponent for two-dimensional percolation. *Physical Review E*, 83(2):020107, February 2011.
- [86] A. Aharony and J. Asikainen. Fractal dimensions and corrections to scaling for critical Potts clusters. *Fractals*, 11(supp01):3–7, February 2003.
- [87] J. Asikainen, A. Aharony, B. B. Mandelbrot, E. Rausch, and J.-P. Hovi. Fractal geometry of critical Potts clusters. *The European Physical Journal B - Condensed Matter*, 34(4):479–487, August 2003.
- [88] W. H. Press, S. A. Teukolsky, W. T. Vetterling, and B. P. Flannery. *Numerical Recipes: The Art of Scientific Computing*. Cambridge University Press, 3rd edition, 2007.

---

## ACKNOWLEDGEMENTS

---

**T**HE WORK PRESENTED in this thesis was performed at the Centre for Nonlinear Studies (CENS) in the Institute of Cybernetics at the Tallinn University of Technology (TTÜ). I would like to thank my supervisor professor Jaan Kalda for his continued support and encouragement to finish this work.

I would also like to thank my brother Marek Mandre and the Department of Computer Engineering at TTÜ for providing computational resources.

This work was supported by Estonian Science Foundation Grant No. 7909, Estonian Science Targeted Project No. SF0140077s08, and EU Regional Development Fund Centre of Excellence TK124.

The scientific methods, mathematical techniques and probability theory studied during the course of this work were applied at Starship Technologies to develop mapping and localisation technology for self-driving delivery robots.

---

## ABSTRACT

---

### ON STATISTICAL TOPOGRAPHY OF SELF-AFFINE SETS

**T**HE WORK IN THIS THESIS investigates fractal structures and is divided into three published articles.

The percolation problem studies clusters formed by randomly connected small objects (or cavities in porous rocks). Once the probability of a location being occupied by an object is increased above a critical threshold, an infinite cluster forms, and connectivity property of the material goes through a second order phase transition. The connected clusters, near criticality, are fractal, and can be characterised by fractal dimension numbers. Further fractal objects can be derived from a cluster – for the two-dimensional percolation its outline, called the hull of the cluster, and the outline of the cluster that excludes narrow gaps, called the unscreened perimeter. The percolation problem also exhibits universality, small random distortions in the cluster structure do not change the fractal dimension numbers or other critical exponents.

Long-range correlations in object placement can change the universality class meaning the fractal dimension numbers change. We assume a correlation function  $c(\rho) \propto |\rho|^{2H}$  ( $-3/4 < H < 0$ ) and perform a Monte-Carlo calculation to determine the fractal dimensions of the hull and the unscreened perimeter. The model can be further generalised to include self-similar processes as generating functions of the percolation clusters extending the calculation range to  $-3/4 < H < 1$ .

Monte-Carlo calculations of the fractal scaling exponents (called the fractal dimensions) are generally done using a finite simulation lattice. The finiteness of the calculation causes distortions in the result called finite-size effects. We develop a method to compensate for a common form of these finite-size effects in Monte-Carlo calculations. The method makes a series of assumptions, while also providing a framework to test them. A way to calculate the statistical uncertainty of the result is also provided. We test the method by calculating the fractal dimension of the hull of the two-dimensional uncorrelated percolation clusters and show that it provides superior results at small lattice sizes (corresponding to computational needs of the calculation) compared to traditional method.

Finally, we investigate finite intersections of moving fractal sets. The mass of such intersection, as a function of relative movement between the two sets, is

found to be self-affine and an analytical relation for its scaling exponent is derived. The formula is tested in a Monte-Carlo fashion on a series of synthetically generated fractals intersecting with a moving line or each other.

---

## KOKKUVÕTE

---

### ENESEAFIINSETE HULKADE STATISTILISEST TOPOGRAAFIAST

**K**ÄESOLEV TÖÖ uurib fraktaalsete objektide omadusi ja on jagatud kolme avaldatud artikli vahel.

Perkolatsiooniprobleem käsitleb juhuslikult paiknevate väikeste objektide (või poorses kivis olevate tühimike) kokkupuutest tekkivate struktuuride (klastrite) omadusi. Kui ühendava objekti esinemise tõenäosus materjali igas punktis tõuseb üle teatud kriitilise piiri, öeldakse, et tekib lõpmatu klaster, ja materjali läbilaskvus läbib faasisiirde. Antud kriitilisel piiril on tekkinud klastrid fraktalid ja neid saab iseloomustada fraktaalse dimensiooninumbriga. Klastritest saab tuletada ka täiendavaid fraktaalseid struktuure – kahedimensionaalse perkolatsiooni korral moodustab klastrite äär (koorik) fraktaalse joone; lisaks eemaldades koorikust kitsad eendid, tekib uus struktuur, mida kutsume väliseks perimeetriks. Perkolatsiooniprobleemile on omane ka universaalsus – häired ühendavate objektide esinemise struktuuris, mis on oma distantsilt (korrelatsiooni kauguselt) piiratud, ei mõjuta dimensiooniarve ega teisi kriitilisi eksponente.

Kui ühendavate objektide paiknemises esineb pikaulatuslikke korrelatsioone, muutub tekkinud klastrite universaalsusklass – fraktaalsed dimensiooninumbriid muutuvad. Antud töös uurime korrelatsioonifunktsiooni  $c(\rho) \propto |\rho|^{2H}$  ( $-3/4 < H < 0$ ) ja teeme Monte-Carlo arvutuse, et leida kahedimensionaalse perkolatsiooniklastrite kooriku ja välise perimeetri fraktaalsed dimensiooninumbriid sõltuvalt parameetrist  $H$ . Mudelit saab lisaks üldistada kaasates enese-sarnased protsessid ja laiendades arvutusvahemiku intervalli  $-3/4 < H < 1$ .

Monte-Carlo arvutused sooritatakse mudelil, mis moodustab regulaarse struktuuri ja lõpliku suurusega võre. Antud arvutusmudeli lõplik suurus põhjustab tulemusel moonutusi, mida nimetatakse lõpliku suuruse efektiks. Me töötame välja meetodi nende moonutuste modelleerimiseks ja lõpmatu klastrite dimensiooniarvu täpseks arvutuseks. Antud meetod eeldab otsitud suuruselt mitmeid omadusi, samas pakub ka viisi nende omaduste olemasolu kontrollida ja annab lisaks tulemuse statistilise määramatuse. Me katsetame antud meetodit arvutades kahedimensionaalse ilma korrelatsioonideta perkolatsiooniklastrite kooriku fraktaalse dimensiooninumbri ja näitame, et antud meetod annab palju täpsema tulemuse võrreldes klassikalise meetodiga väikestel arvutusmudeli suurusel (mis vähendab vastavalt ka arvutusmahukust ja aega).

Lisaks uurime lõpliku suurusega fraktaalsete struktuuride lõigete omadusi juhul kui antud struktuurid liiguvad teineteise suhtes. Antud lõigete mõõt kui funktsioon kahe struktuuri suhtelisest positsioonist on eneseafinne ja me leiame teda iseloomustava eksponendi analüütilise kuju. Antud valemit katsetame erinevate sünteetiliselt genereeritud fraktaalsete struktuuride lõikel kas joonega või omavahel kasutades Monte-Carlo meetodit.

---

## APPENDIXES

---

### PUBLICATION I

I. Mandre, J. Kalda. Monte-Carlo study of scaling exponents of rough surfaces and correlated percolation. *The European Physical Journal B*, 83(1):107-113 (2011).



# Monte-Carlo study of scaling exponents of rough surfaces and correlated percolation

I. Mandre<sup>a</sup> and J. Kalda

Institute of Cybernetics at Tallinn University of Technology, Akadeemia tee 21, 12618, Tallinn, Estonia

Received 20 May 2011

Published online 15 September 2011 – © EDP Sciences, Società Italiana di Fisica, Springer-Verlag 2011

**Abstract.** We calculate the scaling exponents of the two-dimensional correlated percolation cluster's hull and unscreened perimeter. Correlations are introduced through an underlying correlated random potential, which is used to define the state of bonds of a two-dimensional bond percolation model. Monte-Carlo simulations are run and the values of the scaling exponents are determined as functions of the Hurst exponent  $H$  in the range  $-0.75 \leq H \leq 1$ . These results are required by a range of applications (e.g. two-dimensional turbulent transport), for which the scaling exponents are expressed via the hull's fractal dimension.

## 1 Introduction

The world around us is chaotic and seemingly random, but one can still find regularities. Take mountain ranges – these irregular jagged structures may seem intractable to analysis, but often display an interesting property – they look the same at different length scales – they are self-similar. This phenomenon is not limited to the surface features of planets, but is also found in many other places – deposited metal films [4], ripple-wave turbulence [5], crack fronts in material science [6–8], cloud perimeters [9], passive tracers in two-dimensional fluid flows [10–13], etc.

The analysis of these physical systems is often reduced to determining the scaling exponents characterizing the rough surfaces involved. For example, the convective-diffusive transport of a passive scalar in a random two-dimensional steady flow is determined by the scaling exponents of the isolines of the underlying stream-function [12]. Another example is provided by the invasion percolation in fracture landscapes: the scaling laws describing the invasion process depend on the fractal dimensions of the underlying landscapes [14,15].

The aim of this paper is to numerically calculate the values of the scaling exponents of the hull and the unscreened perimeter (defined in the next section) depending on the roughness parameter  $H$ . In Section 2, we start off by giving an overview of the concepts used – rough surfaces and percolation clusters, what we mean by correlations, and a mapping between the two classes of models. Numeric calculations are done through the Monte-Carlo simulations using the two-dimensional bond percolation model; the procedure is described in Section 3. Interpretation of the resulting data requires overcoming the finite

size effects and the convergence problems, which is the subject of Section 4. Finally, Section 5 provides a brief summary of the results and a future outlook for the studies of the statistical topography of random surfaces.

## 2 Overview

**Rough surfaces.** Let  $\psi(x, y) \equiv \psi(\mathbf{r})$  be the height or potential of a self-similar random two-dimensional surface. We define the roughness exponent  $H$  – also known as the Hurst exponent – through the surface height drop at distance  $a = |\mathbf{a}|$  [16]:

$$\langle [\psi(\mathbf{r}) - \psi(\mathbf{r} + \mathbf{a})]^2 \rangle \propto |\mathbf{a}|^{2H}, \quad (1)$$

where angular braces denote averaging over the coordinate  $\mathbf{r}$  (or also over an ensemble of surfaces). This scaling law assumes that  $a_0 \leq |\mathbf{a}| \leq a_1$ , where  $a_0$  and  $a_1$  are the lower and upper cut-off scales, and  $0 \leq H \leq 1$ . Relation (1) also describes self-similarity – the height of a “hill” on the surface is a power law of its diameter, so hills at different scales have the same proportions.

A more generic description, which is not limited to the positive values of  $H$ , can be given through the power spectrum  $P_{\mathbf{k}}$  [17]. We assume that

$$\langle \psi_{\mathbf{k}} \rangle = 0, \quad \langle \psi_{\mathbf{k}} \psi_{\mathbf{k}'} \rangle = P_{\mathbf{k}} \delta_{\mathbf{k} + \mathbf{k}'}, \quad (2)$$

and define the spectral density  $P_{\mathbf{k}}$  as a power law:

$$P_{\mathbf{k}} \propto |\mathbf{k}|^{-2H-2}, \quad \text{for } |\mathbf{k}| \ll a_0^{-1}. \quad (3)$$

This also allows us to conveniently divide the “multiscale” potential  $\psi(\mathbf{r})$  into a sum of “monoscale” functions,

$$\psi(\mathbf{r}) = \sum_{\lambda_i = 2^i \lambda_0} \psi_{\lambda_i}(\mathbf{r}), \quad (4)$$

<sup>a</sup> e-mail: indrek@mare.ee

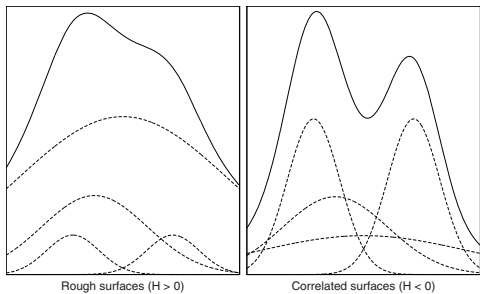


**Fig. 1.** The potential (4) is made up of components with different amplitudes. The amplitude of a component of scale  $\lambda$  is proportional to  $\lambda^H$ . For  $H > 0$  the wider “hills” start to dominate the landscape and once  $H \geq 1$  only the widest “hill” matters. Conversely, for  $H < 0$  local fluctuations start to gain in influence and once  $H < -0.75$  the wider hills lose any influence on the scaling exponents of the surface.

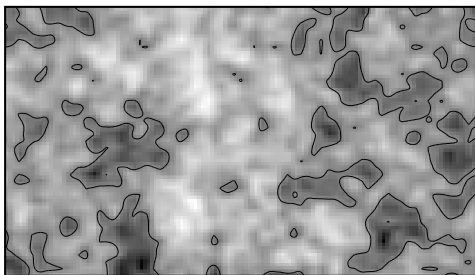


**Fig. 2.** An example of a two-dimensional correlated random potential (here for  $H = 0$  and so  $D_h = 1.5$  [1,2]) with isolines separating the area into “land” and “sea”. The correlations specified by  $H > -1$  lead to potentials that are similar to  $1/f$ -like noise as opposed to uncorrelated “completely” random potentials (at  $H = -1$ ) that resemble white noise (constant power spectrum) [3].

where each component in the sum represents a function with a single characteristic length. The effect of the parameter  $H$  on the amplitude of the “monoscale” components of the “multiscale” potential can be seen in Figure 1.

The random potential  $\psi$  can be also characterized through a correlation function (covariance, assuming  $\langle \psi(\mathbf{x}) \rangle = 0$ )

$$C(\mathbf{a}) = \langle \psi(\mathbf{x})\psi(\mathbf{x} + \mathbf{a}) \rangle. \quad (5)$$

Indeed, for potentials conforming to (3), it is a power law

$$C(\mathbf{a}) \propto |\mathbf{a}|^{2H} \quad a_0 \ll |\mathbf{a}| \ll a_1, \quad (6)$$

which is valid for the range  $-3/4 \leq H \leq 0$ .

With a specific height  $h$ , the random potential defines a set of isolines  $\psi(\mathbf{r}) = h$  (see Fig. 2 for an example). The height  $h$  can be interpreted as the “sea level”. So, a single isoline can be looked at as the coastline of an island or a lake. The coastline is also a self-similar structure, and one can quickly run into difficulties when trying to

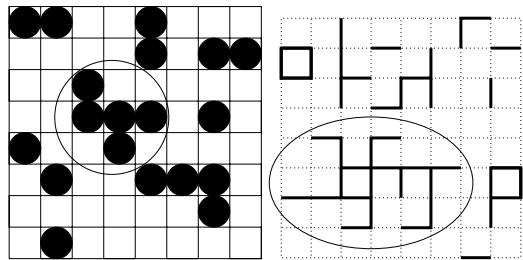


**Fig. 3.** Examples of regular percolation lattices. Square lattice site model to the left and square lattice bond model to the right. Largest clusters have been circled.

measure its length – the result depends on the size of the measuring stick used [18]. The parameter that best characterizes isolines is their scaling exponent – also called their fractal dimension  $D_h$  – which is a fractional number. The length of a coastline can then be given through

$$\langle L(\lambda) \rangle \propto \lambda^{1-D_h}, \quad (7)$$

where  $\lambda$  is the size of the measuring stick.  $D_h$  is a nontrivial function of the underlying surface’s Hurst exponent:

$$D_h = D_h(H). \quad (8)$$

Alternatively, we can take two points at a distance  $a$  on a coastline, and calculate the length of the line between them, assuming a fixed measuring stick  $\lambda = \lambda_0$ :

$$\langle L(a) \rangle \propto a^{D_h}. \quad (9)$$

**The percolation problem** is concerned with the structures that form by randomly placing elementary geometrical objects (spheres, sticks, sites, bonds, etc.) either freely into continuum, or into a fixed lattice (Fig. 3). Two objects are said to communicate, if their distance is less than some given  $\lambda_0$ , and communicating objects form bigger structures called clusters. Percolation theory studies the formation of clusters and their properties. The more interesting aspect is when and how is an infinite cluster formed. This depends on the lattice site occupation probability  $\eta$ . The minimum site occupation probability when an infinite cluster appears is called the percolation threshold  $\eta_c$ . Near this probability, the percolation model displays a critical behavior and long-range correlations.

Percolation theory is used to study and model a wide variety of phenomena: from a fluid flow in a porous medium to thermal phase transitions and critical behavior in magnetism with dilute Ising models.

Several structures can be identified in conjunction with a percolation cluster. For example, the cluster itself, the hull and the unscreened perimeter (Fig. 4). Aside from these, many others are known such as the oceanic coastline [19], the backbone, the chemical (shortest) distance, etc. Near the percolation threshold, all of these structures are fractals and can be characterized by scaling exponents.

Looking at a percolation cluster and an isoline of a random potential, we can identify similar structures: one

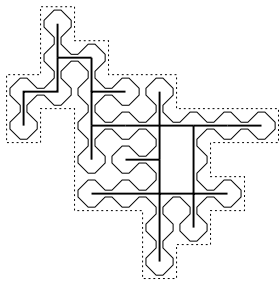


**Fig. 4.** An example square bond percolation cluster. The cluster is made up of the bold segments, the zig-zag is the hull and the dashed line is the unscreened perimeter.

can look at the percolation cluster as an island and its hull as the coastline of the island. This idea will be fleshed out in more precise terms farther below, where a mapping between the two models is described.

One very important and useful aspect about the scaling exponents is a phenomenon known as universality [17] – within specific universality classes, the scaling exponents take the same value across different percolation models. More specifically, they are invariant to small fluctuations or distortions in the lattice structure (for instance, decaying exponentially to distance). This means that the scaling exponents for both the random square bond lattice, and the random square site lattice are the same: both models belong to the same universality class of the two-dimensional uncorrelated percolation.

**Correlated percolation.** Percolation lattice does not need to be completely random, but can entail certain correlations. Here we describe the percolation lattice through an infinite set of random variables  $\theta_i$  which are unity at occupied sites and zero at empty sites ( $i$  denotes the site number). Then we can characterize the correlations through the correlation function

$$c_\theta(\mathbf{x}_i - \mathbf{x}_j) = \langle \theta_i \theta_j \rangle - p^2, \quad (10)$$

where  $p = \langle \theta_i \rangle$  is the site occupation probability.

Alternatively [20], correlations can be brought into the percolation model by assigning each lattice site a random number  $p_i \in [0, 1]$  where  $\langle p_i \rangle = p$ . The site values are then calculated as

$$\theta_i = \Theta(p_i - r_i), \quad (11)$$

where  $\Theta(x)$  is the Heaviside step function and  $\{r_i\}$  are independent random variables uniformly distributed in  $[0, 1]$ . The correlation function is

$$c_p(\mathbf{x}_i - \mathbf{x}_j) = \langle p_i p_j \rangle - p^2 \quad (12)$$

and putting (11) into (10) yields us  $c_\theta(\mathbf{a}) = c_p(\mathbf{a}) \equiv c(\mathbf{a})$  [17].

We are interested in algebraically decaying correlations so that

$$c(\mathbf{a}) \propto |\mathbf{a}|^{2H}, \quad H \leq 0. \quad (13)$$

It is believed [17] that the scaling exponents are determined by the two-point correlation function. This means

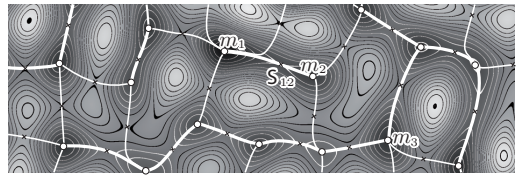


**Fig. 5.** Mapping between the random surfaces and the percolation problem. The bond between two maxima  $m_1$  and  $m_2$  is connecting, if the saddle point  $S_{12}$  on them is above the flood level. So, saddle points are mapped into percolation bonds.

that we have a range of universality classes identified by the parameter  $H$ . One can show that at  $H < -3/4$ , the model belongs to the universality class of uncorrelated percolation [20,21]. However, in the range  $-3/4 \leq H \leq 0$ , the correlations do affect the scaling exponents. We conjecture that the short-range (local) deviations in the percolation lattice do not affect the scaling exponents, and so they are only dependent on the long-range correlations expressed through  $H$  and not on the fine structure of the percolation lattice. For  $H > 0$ , we can argue this by observing that the short-range fluctuations have less impact on the value of the random potential than the long-range correlations and can be diminished by simply scaling the model (see below on the mapping between the random potential and the percolation model).

**There exists a simple mapping** between the rough surfaces and the percolation model [22,23]. According to it, the local maxima of the potential define the lattice sites and the lattice bonds are obtained by drawing fastest-ascent paths from all the saddle points (Fig. 5). The surface  $\psi(\mathbf{x})$  is “flooded” at a given level  $h$  and a bond  $i$  is left connecting if the saddle point  $\mathbf{x}_i$  on it is above the water (is land), that is when  $\psi(\mathbf{x}_i) \geq h$ . As a result, we get an irregular two-dimensional lattice; recall that as per universality, small distortions of the lattice should not affect the resulting scaling exponents. With this mapping, we can relate the islands formed at flooding to the resulting clusters, and their coastlines to the hulls of the said clusters. Also, if the surface correlation function (5) is a power law (6), then so is the correlation function (10) for the percolation model (13), where the parameter  $H$  is the same. Due to universality, the scaling exponents of the matching structures are also the same.

The scaling exponents are of interest in many applications so, there is a need to calculate their values depending on the underlying surface’s roughness parameter  $H$ . In Figure 6, we can see the known results (numeric and analytic), and also interpolations and conjectures for the range  $-3/4 \leq H \leq 0$ . Our next task is to run simulations to numerically shed light on these gray areas (the scaling exponents of the hull and the unscreened perimeter). As these exponents behave the same way for the both problems of rough surfaces and correlated percolation, we can calculate them using the model which is the most convenient from the numerical point of view.

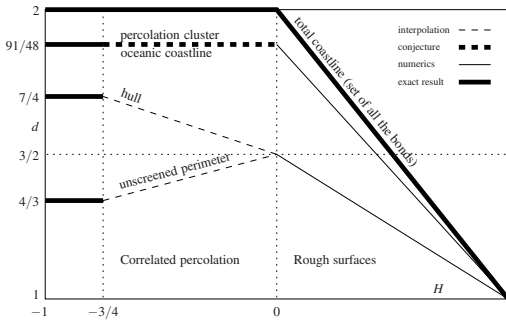


**Fig. 6.** Known results, conjectures and interpolations for the scaling exponents as functions of the Hurst exponent  $H$ . While these functions can be approximated as linear functions, they are in fact non-trivial.

### 3 Monte-Carlo simulations

**Generation of percolation clusters.** We calculate the scaling exponents using the model of correlated two-dimensional bond percolation on square lattices. Our first task is to generate said percolation models so that they conform to the correlation function (13). For this, we first generate random potentials with the requested roughness  $H$ . We take the “flood level” as the value of the potential at some starting location  $\mathbf{x}_0$ , so that  $h = \psi(\mathbf{x}_0)$ , and use it to map the random surface model into one of the percolation models. This is done by overlaying the percolation lattice on the rough surface and calculating the bond values using the Heaviside step function as

$$\theta_i = \Theta(\psi(\mathbf{x}_i) - \psi(\mathbf{x}_0)). \tag{14}$$

This approach is similar to the one described by equation (11) and preserves the correlation exponent: while it is slightly different from the maxima-saddle point mapping, the differences are observable only at the smallest scales (of the order of the bond length); one can expect that these short-scale differences do not affect the scaling exponents. Indeed, it has been shown that in the case of uncorrelated percolation lattices, such short-scale differences leave the scaling exponents intact [20]; it is natural to conjecture that the same universality holds also for the correlated percolation problem with  $H > -0.75$  (c.f. Sect. 2). Using the potential as the underlying model allows us to get the results in the parameter range  $-0.75 \leq H \leq 1$ .

**To generate random potentials,** we exploit formula (4). We generate different components (layers) of the potential for different lengths and sum them up. The  $i$ -th layer  $\psi_{\lambda_i}(\mathbf{r})$  is formed by a grid of cells, where the grid cell side length is  $2^i$ , and at the center of each cell  $j$  we place a cone of height  $r_j 2^{iH}$ , where  $r_j$  is an independent uniform random variable in the range  $[-0.5, 0.5]$  (Fig. 7). The cones have a diameter of  $3\lambda_i$ , so the resulting overlap yields a smoother potential. However, the overlap or the shape used (cone, in this case) does not significantly affect how fast the results converge to the asymptotic power laws. So, one can choose a shape more optimized for the

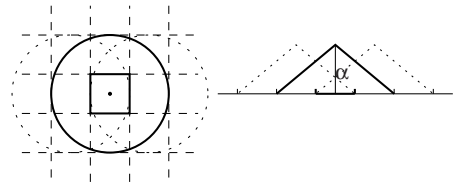


**Fig. 7.** For the  $i$ -th layer  $\psi_{\lambda_i}(\mathbf{r})$  in (4), we divide space into a grid of cells with side length of  $\lambda_i = 2^i$  ( $\lambda_0 = 1$ ). At the center of each cell  $j$ , a cone is placed with height  $\alpha_j = r_j 2^{iH}$ , where  $r_j$  is an independent uniform random variable in the range  $[-0.5, 0.5]$ . The cones have a diameter of  $3\lambda_i$  and so overlap.

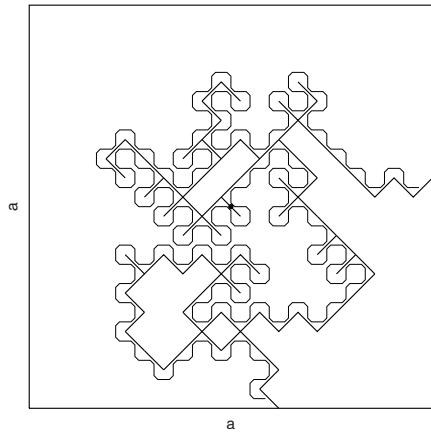


**Fig. 8.** Calculating the length of a hull for size  $a$ . We start from the center of a  $a \times a$  box and dynamically calculate bond values as we trace the hull until reaching the side of the box. We discard hulls that make a full circle. The box sizes picked are  $a = 8, 16, 32, \dots, 1024, \dots$

speed of numerical calculations (for instance, one could use a simple block or a cylinder). The number of layers required depends on the value of  $H$ . For example, at  $H = 0$ , we can work with  $i = 0 \dots 30$ .

**Gathering data** is a matter of generating percolation clusters of different sizes and tracing the structures of interest within these. For the hull, this is done in the following way. We constrain ourselves to a  $a \times a$  box, and start to dynamically trace the hull from the center point  $\mathbf{x}_0$  until it reaches any sides of the box (Fig. 8). Hulls that make a full circle are discarded. To get additional data, we also trace backwards from the center, so that the both ends of the hull reach the box’s sides. We do this millions of times for differently sized boxes  $a = 8, 16, \dots, 1024, \dots$ . While for some cases, the range of values  $a = 8, 16, \dots, 512$  is sufficient, slow convergence in some regions of  $H$  forces us to use larger lattices. However, the size is limited by computational resources and in our case it was not practical to go over  $a = 2048$ .

Once we have a hull, we want to measure its size (length). While the easiest way would be to just sum the number of segments in the trace line, it is also possible

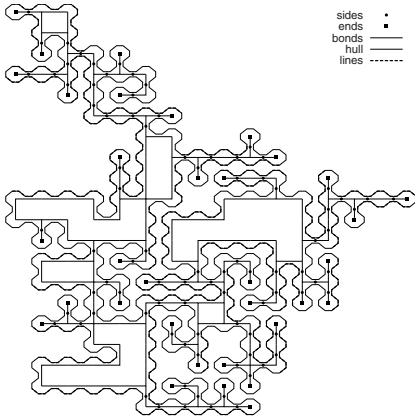


**Fig. 9.** Counting the size of the hull can be done in many ways. One can simply count the number of segments (hull), the number of bonds the hull touches from both sides (sides), the total number of bonds the hull touches (bonds), the number of times a single bond sticks out (ends), or the number of times the hull forms a straight line of 4 segments (lines). All of these scale with the same power law.

to determine the size by other properties (Fig. 9). All of these properties scale with the same power law. We can denote the size of a single hull as  $L_i(a_j)$ , where  $i$  indicates the property. As this is different for each individual hull, we find the average value

$$\mathcal{L}_i(a_j) = \langle L_i(a_j) \rangle, \quad (15)$$

and as per equation (9), this should scale as a power law with the exponent  $D_h$ . However, the scaling is asymptotic ( $a \rightarrow \infty$ ), so for finite  $a$ , there are sizable deviations called finite size effects. These come from the geometry and finite size of the lattice. Using (9), we can estimate the exponent as

$$\tilde{D}_h(\sqrt{a_j a_{j-1}}) \simeq \ln_2 \frac{\mathcal{L}(a_j)}{\mathcal{L}(a_{j-1})} \quad (a_j = 2a_{j-1}). \quad (16)$$

Plotting this for the uncorrelated percolation (Fig. 10), we can see how the different properties converge towards the value  $D_h = 7/4$ . The finite size effects are strongly manifested for the smaller lattices.

## 4 Data analysis

**To calculate the scaling exponents** from the data, the following assumptions are made:

1. the mathematical expectation for each property can be described as an infinite series

$$\bar{L}_i(a) = \sum_{\mu=1}^{\infty} A_{i\mu} a^{\alpha_{i\mu}}, \quad \alpha_{i(\mu+1)} < \alpha_{i\mu}, \quad (17)$$

where  $i = 1, \dots, m$ ;

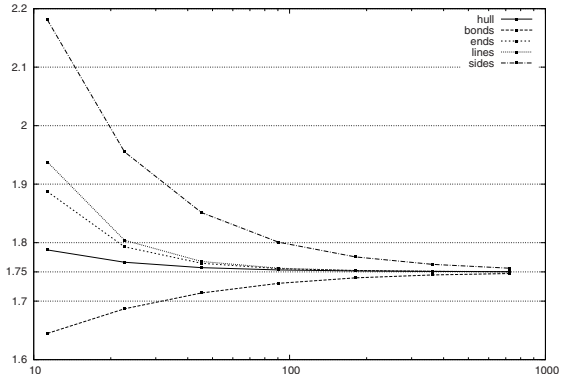


**Fig. 10.** Convergence of the hull properties for the uncorrelated percolation (towards  $D_h = 7/4 = 1.75$ ).

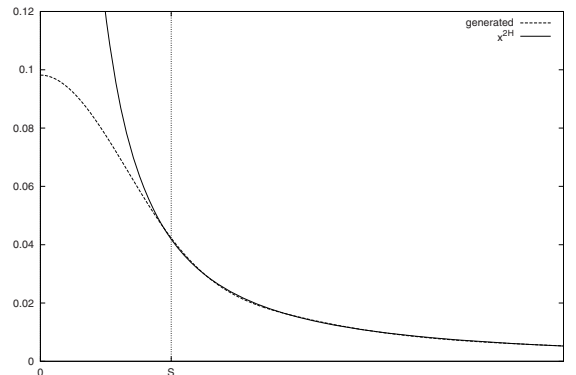


**Fig. 11.** Covariance of a potential versus the power law  $x^{2H}$ . Here  $S$  marks the length at which the covariance starts to diverge from the power law.

2.  $\alpha_{i\mu} \equiv \alpha_\mu$  for  $\mu = 1, \dots, m$ ;
3. the leading terms in the sum are linearly independent ( $\det \|A_{\mu i}\| \neq 0$ ).

After these assumptions, we apply a variation of the least squares method described in [24] and previously used in [19]. The method works if the assumptions made are correct (the method also validates them) and yields us the value  $\alpha_1$ , which is the scaling exponent we are looking for. So, the reason why we counted all the different properties for the hull (Fig. 9), is that they are necessary for this method.

For the unscreened perimeter, a similar approach is taken. The unscreened perimeter is obtained by taking a hull but pruning it from “fjords”.

**Convergence problems.** In some areas the calculations are hindered by very slow convergence. Let parameter  $S$  represent the length at which the covariance of the generated potential starts to differ from that of the ideal  $|a|^{2H}$  law:

$$S = 3 \times 2^{s-1}, \quad (18)$$

where  $s$  indicates the smallest-scale layer index (Fig. 11). When  $S$  decreases (by adding bottom layers), local

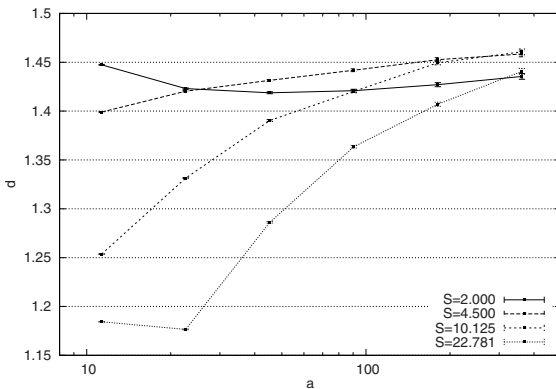


**Fig. 12.** Convergence of a property of the unscreened perimeter at  $H = 0$  (towards theoretically known  $D_u = 1.5$ ) for different values of parameter  $S$ .

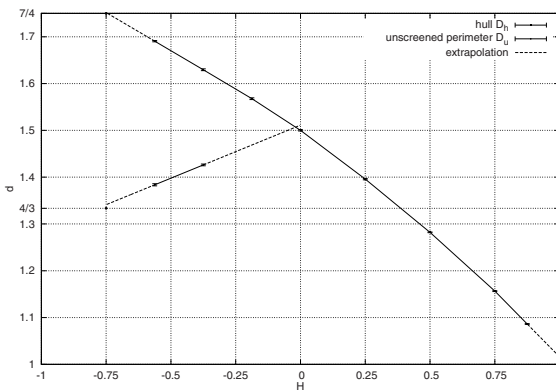


**Fig. 13.** Scaling exponents of the hull and the unscreened perimeter as functions of the Hurst exponent  $H$ . Data points for the positive side of  $D_u$  are not plotted as to avoid clutter.

fluctuations start to gain in influence compared to those of the long-range correlations. This causes a strong finite-size effect and the scaling exponents behave as if  $H$  was smaller (Fig. 12). Conversely, when increasing  $S$ , the scaling exponents can initially behave as if  $H$  was greater than it really is.

To get over these distortions, one could calculate for bigger lattice sizes. But often this is not an option as convergence can be very slow and computational resources are limited. Another way would be to manually find the optimal layer configuration that minimizes distortions. This is the approach we took and yielded good results for the hull (aside from the values  $H = -0.75$  and  $H = +1.00$ ). However, the convergence of the unscreened perimeter is very sensitive to changes in the layer configuration and for most data points did not yield clear results.

**The results** can be seen in Figure 13 and Table 1. The hull behaves as expected. While it did not yield clear results at  $H = -0.75$  and  $H = 1.00$ , the extrapolations provided seem to indicate that it terminates at  $7/4$  and 1

**Table 1.** Numeric results for the hull and the unscreened perimeter (0.95 confidence).

H	$D_h$	$D_u$
1.0000		
0.8750	$1.0862 \pm 0.0008$	$1.0862 \pm 0.0022$
0.7500	$1.1565 \pm 0.0010$	$1.1565 \pm 0.0011$
0.5000	$1.2820 \pm 0.0008$	$1.2820 \pm 0.0011$
0.2500	$1.3958 \pm 0.0014$	
0.0000	$1.5000 \pm 0.0013$	
-0.1875	$1.5676 \pm 0.0018$	
-0.3750	$1.6295 \pm 0.0019$	$1.4261 \pm 0.0018$
-0.5625	$1.6906 \pm 0.0014$	$1.3837 \pm 0.0023$
-0.7500		

respectively. Due to the convergence problems, the results for the unscreened perimeter are not as clear. However, one can say that at least that the result do not contradict the analytical findings and support the applicability of a nearly-linear interpolation between the points  $D_u(0) = 1.5$  and  $D_u(-3/4) = 4/3$ .

## 5 Conclusion

We have run Monte-Carlo simulations to determine the scaling exponents of the hull and the unscreened perimeter as functions of the Hurst exponent in the range  $-0.75 \leq H \leq 1$ . For this, we first generated random potentials conforming to the required correlation function by summation of component potentials of different characteristic lengths and mapping the potential into percolation models. Hulls and unscreened perimeters were traced from these models, and their lengths calculated for different scales. A variation of the least squares method was used to obtain the values of the exponents.

The results confirm the previously known data in the range  $0 \leq H \leq 1$  and also the conjectures for the behavior in the range  $-0.75 \leq H \leq 0$ , see Figure 13. The particular results regarding the fractal dimension  $D_h(H)$  of hulls confirm that for  $0 \leq H \leq 1$ , the 4-vertex model (i.e. the rough surfaces in 1+1-dimensional geometry) [25] belongs to the same universality class as the isotropic Gaussian self-affine surfaces (assuming the respective equality of the Hurst exponents). Indeed, comparing the numerical results of reference [25] and those of the current study shows that for the entire range of  $0 \leq H \leq 1$ , the values of  $D_h(H)$  coincide within the uncertainties of  $ca 10^{-3}$ . An important consequence is that the conjecture about the super-universality of the loop correlation exponent  $x_l(H) \equiv \frac{1}{2} [1,2]$  (which has been exploited in several studies, cf. [26–29]) is clearly rejected: this conjecture implies  $D_h(H) = \frac{3}{2} - \frac{H}{2}$ , which falls well beyond the uncertainty margins of the present simulation results (for instance, at  $H = \frac{1}{2}$ , the conjectured value  $\frac{5}{4}$  falls far from the range of  $1.2820 \pm 0.0008$ ).

The obtained results are valuable for a range of practical applications (such as the turbulent transport in quasi-stationary velocity fields), for which the scaling exponents have been analytically expressed via the fractal dimension

of the hull. As a future outlook, our method can be applied to calculate other scaling exponents of the correlated percolation problem and statistical topography, such as the fractal dimensions of the clusters (oceanic coastlines), percolation backbone, etc. It can be also extended to study the scaling laws of the transport on quasi-stationary velocity fields.

This work was supported by Estonian Science Targeted Project No. SF0140077s08 and Estonian Science Foundation Grant No. 7909.

## References

1. J. Kondev, C.L. Henley, Phys. Rev. Lett. **74**, 4580 (1995)
2. J. Kondev, C.L. Henley, D.G. Salinas, Phys. Rev. E **61**, 104 (2000)
3. A. Hansen, J. Schmittbuhl, G. Batrouni, Phys. Rev. E **63**, 062102 (2001)
4. G. Palasantzas, J. Krim, Phys. Rev. Lett. **73**, 3564 (1994)
5. W.B. Wright, Science **278**, 1609 (1997)
6. E. Bouchaud, G. Lapasset, J. Planès, S. Naveos, Phys. Rev. B **48**, 2917 (1993)
7. S. Santucci, K.J. Måløy, A. Delaplace, J. Mathiesen, A. Hansen, J.Ø.H. Bakke, J. Schmittbuhl, L. Vanel, P. Ray, Phys. Rev. E **75**, 016104 (2007)
8. J.Ø.H. Bakke, A. Hansen, Phys. Rev. Lett. **100**, 045501 (2008)
9. J.D. Pelletier, Phys. Rev. Lett. **78**, 2672 (1997)
10. H.J. Catrakis, P.E. Dimotakis, Phys. Rev. Lett. **77**, 3795 (1996)
11. J. Kondev, G. Huber, Phys. Rev. Lett. **86**, 5890 (2001)
12. M. Isichenko, J. Kalda, J. Nonlinear Sci. **1**, 375 (1991)
13. D. Bernard, G. Boffetta, A. Celani, G. Falkovich, Phys. Rev. Lett. **98**, 024501 (2007)
14. J. Schmittbuhl, A. Hansen, H. Auradou, K.J. Måløy, Phys. Rev. E **61**, 3985 (2000)
15. H. Auradou, K.J. Måløy, J. Schmittbuhl, A. Hansen, D. Bideau, Phys. Rev. E **60**, 7224 (1999)
16. B.B. Mandelbrot, *The Fractal Geometry of Nature* (Freeman, New York, 1982)
17. M.B. Isichenko, Rev. Mod. Phys. **64**, 961 (1992)
18. B. Mandelbrot, Science **156**, 636 (1967)
19. J. Kalda, Europhys. Lett. **84**, 46003 (2008)
20. A. Weinrib, Phys. Rev. B **29**, 387 (1984)
21. A. Harris, J. Phys. C Solid State Phys. **7**, 1671 (1974)
22. J.M. Ziman, J. Phys. C **1**, 1532 (1968)
23. A. Weinrib, Phys. Rev. B **26**, 1352 (1982)
24. J. Kalda, [arXiv:0804.1911v1](https://arxiv.org/abs/0804.1911v1) (2008)
25. J. Kalda, Phys. Rev. E **64**, 20101 (2001)
26. M.A. Rajabpour, S.M. Vaez Allaei, Phys. Rev. E **80**, 011115 (2009)
27. A.A. Saberi, H. Dashti-Naserabadi, S. Rouhani, Phys. Rev. E **82**, 020101 (2010)
28. M.G. Nezhadhighi, M.A. Rajabpour, Phys. Rev. E **83**, 021122 (2011)
29. S.B. Ramisetti, C. Campaña, G. Anciaux, J.F. Molinari, M.H. Müser, M.O. Robbins, J. Phys.: Condens. Matter **23**, 215004 (2011)



PUBLICATION II

I. Mandre, J. Kalda. Efficient method of finding scaling exponents from finite-size Monte-Carlo simulations. *The European Physical Journal B*, 86(2):56 (2013).



# Efficient method of finding scaling exponents from finite-size Monte-Carlo simulations

Indrek Mandre<sup>a</sup> and Jaan Kalda

Institute of Cybernetics at Tallinn University of Technology, Akadeemia tee 21, 12618 Tallinn, Estonia

Received 14 May 2012 / Received in final form 18 October 2012

Published online 18 February 2013 – © EDP Sciences, Società Italiana di Fisica, Springer-Verlag 2013

**Abstract.** Monte-Carlo simulations are routinely used for estimating the scaling exponents of complex systems. However, due to finite-size effects, determining the exponent values is often difficult and not reliable. Here, we present a novel technique of dealing with the problem of finite-size scaling. This new method allows not only to decrease the uncertainties of the scaling exponents, but makes it also possible to determine the exponents of the asymptotic corrections to the scaling laws. The efficiency of the technique is demonstrated by finding the scaling exponent of uncorrelated percolation cluster hulls.

## 1 Introduction

Determining the scaling exponents from the finite-size simulation data is a very common task in the physics of complex systems. In particular, this technique is widely used in the context of phase transitions, surface roughening, turbulence, granular media, etc. (cf. Refs. [1–3]). Typically, such finite-size Monte-Carlo studies involve extrapolation of the simulation data towards infinity. Unless there is some theoretical understanding about the functional form of the finite-size corrections to the asymptotic scaling laws of the particular system, such an extrapolation carries a risk of underestimating the uncertainties. In some cases, it may be helpful to increase the computation time and system size, and optimize the simulation scheme (cf. Ref. [4]). However, this is not always feasible, because the convergence to the asymptotic scaling law may be very slow (cf. Ref. [5]). Additional difficulties arise, when one needs to determine the exponents of the finite-size correction terms (cf. Ref. [6]), or when the asymptotic power law includes a logarithmic pre-factor.

In what follows, we describe a novel technique for determining scaling exponents from the finite-size simulation data. First, we describe in which form the scaling law is expected to hold, and review the traditional method. Then, we introduce the basic idea which allows us to improve qualitatively the precision of the finite-size Monte-Carlo studies, the idea of studying simultaneously multiple physical quantities that asymptotically scale with the same exponent, but have different finite-size correction terms. After that, we describe the novel method to analyze Monte-Carlo simulation data for extracting the scaling exponents and the finite-size correction terms. Finally, we provide an example application of the technique

and find the scaling exponent of the uncorrelated percolation cluster hulls. A comparison is offered with the naive application of fitting to the asymptotic scaling law without considering the finite-size correction terms.

## 2 The asymptotic scaling law

Let us consider a system (possibly idealized, modeling a real one), which is characterized by its size  $x$ , assuming that the smallest possible value of  $x$  plays the role of the unit length.

Further, suppose that the mathematical expectation of a certain physical quantity scales as:

$$\langle L(x) \rangle \propto x^\alpha, \quad x \gg 1; \quad (1)$$

here, the angular braces denote averaging over the full ensemble of the model systems. The Monte-Carlo simulations can be used to estimate the values of the mathematical expectation (1) for several system sizes  $x_1 < x_2 < \dots < x_n$ , denoted as:

$$\mathcal{L}_i \equiv \overline{L(x_i)}, \quad i = 1 \dots n, \quad (2)$$

and the variances of them as  $\sigma_i^2$ ; the bar over a symbol denotes averaging over a set of Monte-Carlo simulations. Then, a least-square fit can be used to obtain the scaling exponent  $\alpha$  (cf. Ref. [2]). However, it is often difficult to estimate the uncertainty of the obtained result, because the magnitude of the finite-size corrections  $\Delta$  within

$$\langle L(x) \rangle = Ax^\alpha + \Delta(x), \quad (3)$$

is unknown. Of course, one can plot  $\ln \mathcal{L}_i$  versus  $\ln x_i$  and determine such a crossover point  $i = k$  that for  $i \geq k$ , the

<sup>a</sup> e-mail: indrek@mare.ee

data points lay within their statistical uncertainties on a straight line. Then, only the data points with  $i \geq k$  will be used for finding the exponent  $\alpha$ . However, one can easily underestimate the adequate value of  $k$ , because the statistical fluctuations just happen to compensate the finite-size corrections  $\Delta$ . On the other hand, taking excessively large values of  $k$  would inflate the variance of the outcome. Finally, in some cases, the decay rate of the corrections  $\Delta$  can be very slow, so that the method outlined above will fail at the first step – there is no linear range of the graph.

To resolve these problems, we are going to make a series of assumptions. Later, we will see that the method we develop here also validates these assumptions as it is applied and so the assumptions do not have to be tested externally.

**First**, we assume a more complex scaling law for the mathematical expectation of the physical quantity  $L$ , in the form:

$$\langle L(x) \rangle = \sum_{k=1}^{\infty} A_k x^{\alpha_k}, \quad (4)$$

assuming that the most significant (in the sense of contributing to the  $\mathcal{L}_i$ ) members of the sum come first. The greatest of the exponents  $\alpha_k$  is the  $\alpha$  we are looking for. We separate  $m$  first members and rewrite the sum as:

$$\langle L(x) \rangle = \sum_{k=1}^m A_k x^{\alpha_k} + \Delta(x). \quad (5)$$

This form for the finite-size correction terms has been used previously (cf. Ref. [7]).

**Second**, we assume that the contribution of  $\Delta$  to  $\mathcal{L}_i$  is smaller than their statistical fluctuation.

Now, we can apply the least-squares fit to search for the  $2m$  parameters,  $A_k$  and  $\alpha_k$ ,  $k = 1 \dots m$ . However, there are a few problems. Unless we have some underlying idea about the parameters, the least-squares search is complicated –  $m$  of the parameters are non-linear and the search space is huge with many local minima. We need at least  $n \geq 2m + 1$  data points, all at different system sizes – increasing computational complexity. Also, we cannot be sure the assumptions we have made so far are actually correct (aside from the chi-square test that is designed to test data probability rather than the model).

### 3 Different physical quantities

Our method is designed to resolve these problems; it will work, if the following third condition is satisfied.

**Third**, we assume that it is possible to find more than one physical quantity with similar scaling behavior. So, we assume that instead of having just one quantity, we can define  $m$  distinct (linearly independent in the finite scale) quantities, the mathematical expectations  $\langle L_j \rangle$  ( $j = 1 \dots m$ ) of which asymptotically scale using the same exponent  $\alpha$ , but also have the same exponents  $\alpha_k$

( $k = 1 \dots m$ , so we have the same number of exponents as physical quantities) for the finite-size correction terms:

$$\langle L_j(x) \rangle = \sum_{k=1}^m A_{jk} x^{\alpha_k} + \Delta_j(x), \quad j = 1 \dots m. \quad (6)$$

We denote  $\mathcal{L}_{ij} \equiv \overline{L_j(x_i)}$  with corresponding covariances  $\Sigma_{ikl} = \text{Cov}(\mathcal{L}_{ik}, \mathcal{L}_{il})$ ; these covariances can be easily calculated during the Monte-Carlo simulations. For each system size, we then have a covariance matrix  $\Sigma_i = (\Sigma_{ikl})_{kl}$ ,  $i = 1 \dots n$ ; with corresponding inverse matrices  $\mathbf{W}_i = \Sigma_i^{-1} = (w_{ijk})_{kl}$ . A least-squares fit can now be done by minimizing

$$\sum_{i=1}^n \sum_{j,k=1}^m \left( \mathcal{L}_{ij} - \sum_{l=1}^m A_{jl} x_i^{\alpha_l} \right) w_{ijk} \left( \mathcal{L}_{ik} - \sum_{l=1}^m A_{kl} x_i^{\alpha_l} \right), \quad (7)$$

which at minimum is of chi-square distribution with  $nm - m^2 - m$  degrees of freedom. We have reduced the necessary calculation complexity as we now only need  $n \geq m + 2$  different system sizes. Further, the distinct physical quantities that scale using the same exponents can be calculated from the same system instance within the Monte-Carlo simulations.

The minimization problem is still non-linear in  $m$  parameters and now with total of  $m^2 + m$  parameters. We found it yields well to the Levenberg–Marquardt algorithm, given proper initial values. However, with inadequate initial values, it can still lead to inconsistent results and local minima.

It is trivial that more data should yield a better result. The third assumption shows how to get this data and how it is done at no extra computational cost. Next, we look into how to consistently apply this “free” data to yield better results.

### 4 Description of the method

To simplify the problem we rewrite equation (6) in matrix form, with  $\mathbf{L} = (\langle L_j(x) \rangle)$ ,  $\mathbf{A} = (A_{jk})$ ,  $\mathbf{X} = (x^{\alpha_k})$ ,  $\mathbf{\Delta} = (\Delta_j(x))$ , and derive

$$\begin{aligned} \mathbf{L} &= \mathbf{A}\mathbf{X} + \mathbf{\Delta}, \\ \mathbf{X} &= \mathbf{A}^{-1}\mathbf{L} - \mathbf{A}^{-1}\mathbf{\Delta} = \mathbf{B}\mathbf{L} + \boldsymbol{\delta}, \end{aligned} \quad (8)$$

where  $\mathbf{B} = \mathbf{A}^{-1}$  and  $\boldsymbol{\delta} = -\mathbf{A}^{-1}\mathbf{\Delta}$ . A single row from this equation is:

$$x^{\alpha_k} = \sum_{j=1}^m B_{kj} \langle L_j(x) \rangle + \delta_k, \quad k = 1 \dots m. \quad (9)$$

We remark here that as  $\Delta_j$  are small, so are the  $\delta_k$ .

We now attempt to find the parameters  $B_{kj}$  by treating this as a least-squares fitting problem. For this, we construct a function:

$$S(d) = \sum_{i=1}^n \frac{\left( x_i^d - \sum_{j=1}^m C_j \mathcal{L}_{ij} \right)^2}{s_i^2}. \quad (10)$$

The weighting factor  $s^2$  is simply the variance of the expression within the parentheses:

$$s_i^2 = \text{Var} \left( x_i^d - \sum_{j=1}^m C_j \mathcal{L}_{ij} \right) = \sum_{kl=1}^m C_k C_l \Sigma_{ikl}. \quad (11)$$

We minimize the function  $S(d)$  in relation to the parameters  $C_1, \dots, C_m$ . Aside from the weighting factor  $s^2$ , that depends on the values  $C_k$ , this is a simple linear-least-squares problem. We found that by initially setting  $C_k$  to 1 and iteratively running the linear-least-squares algorithm, then near the minima of  $S(d)$  the function value converges in three or four iterations.

Considering the assumptions made, it is clear that near  $d = \alpha_k$  the function  $S(d)$  should have a minimum. Conversely, if the function  $S(d)$  has exactly  $m$  clear minima, our assumptions about the scaling law must be correct and values of  $\alpha_k$  are exactly where  $S(d)$  has minima. Hence, we have found a way to extract the values  $\alpha_k$  from the function  $S(d)$ .

For statistical testing, the vectors  $(\mathcal{L}_{i1}, \dots, \mathcal{L}_{im})$ ,  $i = 1 \dots n$  must be of multivariate normal distribution. Satisfying this, at minima the function  $S(d)$  is of chi-square distribution with  $n - m - 1$  degrees of freedom. Consequently, just as with (7), we must have  $n \geq m + 2$ . To accept the exponents  $\alpha_k$  as significant, a chi-square test must be performed: at minima the function  $S(d)$  has to satisfy the relation

$$S(\alpha_k) \leq \chi_{n-m-1}^2(p), \quad (12)$$

where  $\chi_{\text{dof}}^2(p)$  is the quantile at  $p$  of the chi-square distribution with  $n - m - 1$  degrees of freedom (dof).

Aside from the exponents  $\alpha_k$ , we can also find their uncertainties  $\Delta\alpha_k$  from:

$$S(\alpha_k \pm \Delta\alpha_k) = S(\alpha_k) + \chi_1^2(p). \quad (13)$$

Here, we are making use of the constant chi-square boundary as the confidence limit -  $\Delta\alpha_k$  is determined by the width of the dip at the minimum of  $S(d)$ , at level  $S(\alpha_k) + \chi_1^2(p)$ .

In case we are uncertain about the results, we can always revert back to (7). We found that when doing so, the parameters derived using the above described novel method perform flawlessly as initial values for this nonlinear minimization problem and results yielded by the classical but complex (7) are the same.

Compared to (7), where we have a nonlinear multidimensional minimization problem, the novel method contains a linear one-dimensional search. This gives us consistent results as we do not have to deal with local minima. Furthermore, each of the correction exponents is statistically tested separately, instead of one big sum in (7) - we have found that this excludes invalid results that would otherwise pass.

## 5 Example application

As an example of the techniques described, we calculate the scaling exponent of the hull of the uncorrelated

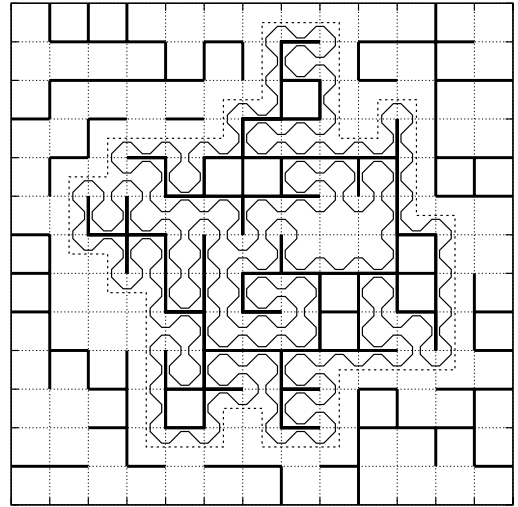


**Fig. 1.** Square bond percolation lattice. Bonds (bold solid line segments) are randomly placed into the lattice. Clusters are formed by bonds that are connected to each other. The largest cluster in the center is illustrated with its hull (the zig-zag line) and the unscreened perimeter (the dotted line).

percolation cluster. The percolation problem deals with the structures that form by randomly placing elementary geometrical objects (spheres, sticks, sites, bonds, etc.) either freely into continuum, or into a fixed lattice (Fig. 1). Two objects are said to communicate, if their distance is less than some given  $\lambda_0$ , and communicating objects form bigger structures called clusters. Percolation theory studies the formation of clusters and their properties. The more interesting aspect is when and how does an infinite cluster form. This depends on the lattice site occupation probability. The minimum site occupation probability when an infinite cluster appears is called the percolation threshold. Near this probability, the percolation model displays critical behavior and long-range correlations. For the square bond percolation model we use here, this critical probability is  $p = 0.5$ .

Percolation theory is used to study and model a wide variety of phenomena, for example fluid flow in a porous medium [8], thermal phase transitions and critical behavior in magnetism with dilute Ising models [9].

Several structures can be identified in conjunction with a percolation cluster. For example, the cluster itself, the hull and the unscreened perimeter (Fig. 1). Aside from these, many others are known such as the oceanic coastline [5], the backbone or the chemical (shortest) distance. Near the percolation threshold, all of these structures are fractals and can be characterized by scaling exponents.

In this example, we concentrate on the scaling exponent of the hull of uncorrelated percolation clusters. The exact value of this scaling exponent is known,  $d_H = 1.75$  [10,11].

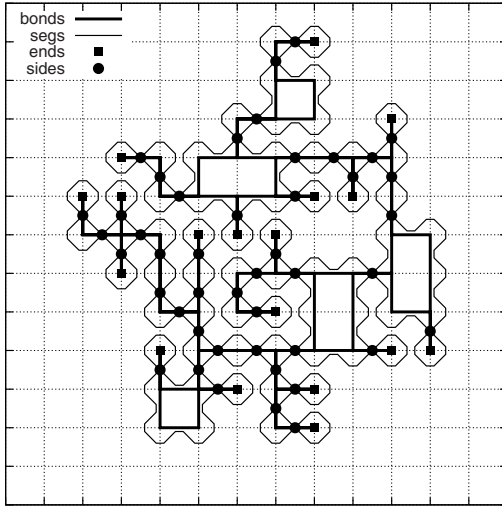


**Fig. 2.** Some of the different physical quantities that scale with the same exponent as the hull.

First, we identify the different physical quantities (from here on, the properties of the hull) that scale together with the hull. They are (see Fig. 2):

- bonds – the number of distinct bonds the hull touches,
- segs – the number of segments in the hull zig-zag,
- ends – the number of distinct bonds touched by the hull that have no connections on one end,
- sides – the number of distinct bonds that are touched by the hull from both sides,
- lines – the number of occurrences of four straight segments in the hull,
- corners – the number of times bonds form corners in the hull,
- ones – the number of unset bonds by the hull that have exactly one set bond connected to them,
- twos – the number of unset bonds by the hull that have exactly two set bonds connected to them,
- threes – the number of unset bonds by the hull that have exactly three set bonds connected to them.

It is possible to visualize how the scaling of these properties converges towards the  $d_H = 7/4$ . From (1),

$$\mathcal{L}_{ij} \simeq C x_i^{\tilde{d}_j}, \quad \mathcal{L}_{(i+1)j} \simeq C x_{i+1}^{\tilde{d}_j}, \quad (14)$$

where  $C$  is some constant. Dividing these two equations yields us:

$$\frac{\mathcal{L}_{(i+1)j}}{\mathcal{L}_{ij}} \simeq \frac{x_{i+1}^{\tilde{d}_j}}{x_i^{\tilde{d}_j}} \Rightarrow \tilde{d}_j \simeq \ln \frac{\mathcal{L}_{(i+1)j}}{\mathcal{L}_{ij}} \bigg/ \ln \frac{x_{i+1}}{x_i}. \quad (15)$$

In simulations one often takes  $x_{i+1} = 2x_i$ , and placing the intermediate exponent at  $\sqrt{x_i x_{i+1}}$ , we get:

$$\tilde{d}_j(\sqrt{x_i x_{i+1}}) = \ln_2 \frac{\mathcal{L}_{(i+1)j}}{\mathcal{L}_{ij}}, \quad (x_{i+1} = 2x_i). \quad (16)$$

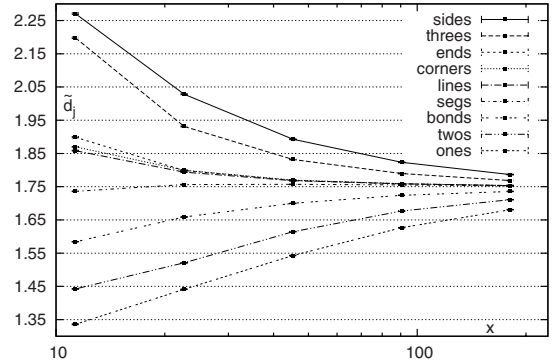


**Fig. 3.** Convergence of the scaling exponents of the hull properties towards  $d_H = 1.75$ .

The convergence of the nine studied properties towards the value  $d_H = 1.75$  can be seen in Figure 3. The finite-size effects are well pronounced for small system sizes. This data is practically unusable for the simple model (3) – there is no linear range for the data values and any attempt will fail at the chi-square test.

Some of the properties converge faster than others. Our method is designed to work even with the very slowly converging properties. Hence, to show its efficacy, out of the nine studied, we have selected the five worst converging properties for what follows (sides, threes, bonds, twos, ones).

We run a Monte-Carlo simulation to gather data (the values  $\mathcal{L}_{ij}$  and  $\Sigma_{ijk}$  where  $i = 1 \dots n$  and  $j, k = 1 \dots m$ ;  $n \geq m + 2$ ). This is done by tracing instances of hulls within the confines of a system-sized box (Fig. 4). The system sizes used were 8, 16,  $\dots$ , 256. At each system size  $4.2 \times 10^6$  different hulls were generated and their properties counted.

Once we have the data, we try out different variations of  $m$  physical quantities and find an instance of  $S(d)$  that matches our requirements (has  $m$  clear minima that all satisfy the chi-square test with  $n - m - 1$  degrees of freedom). One such combination (with  $m = 4$ ) can be seen in Figure 5. The rightmost peak is at the exponent  $\alpha$  we are looking for and we can determine its statistical uncertainty using relation (13).

The number of exponents extractable is unknown, so different values of  $m$  must be tested. The chi-square test at the peaks may fail if the statistical uncertainty in  $\mathcal{L}_{ij}$  is comparable to  $\Delta_j(x_i)$  within equation (6). In such a case we must discard simulated data from the smallest system and possibly run Monte-Carlo simulations for an additional larger system. When discarding smaller systems, the constitution of the first  $m$  members in equation (6) may change – some members may only be significant for the smaller systems. When that happens we may lose one or more of the minima and have to decrease  $m$ . Parameter  $m$  also determines the number of degrees of freedom for the overall system (as we take  $n = m + 2$ ), hence while increasing  $m$  will decrease the contribution of the leftover

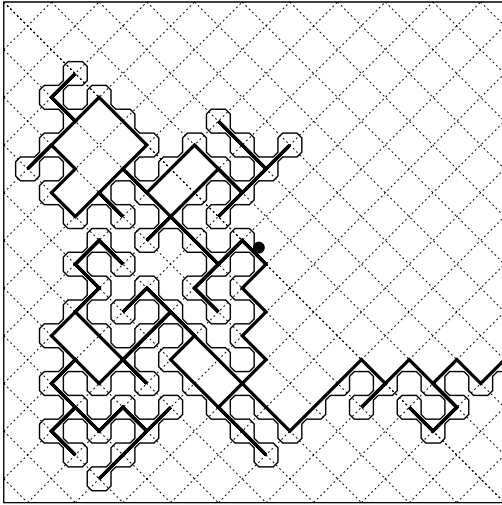


**Fig. 4.** Monte-Carlo simulation system instance for scale length  $x_i$ . We start from the center (marked by a dot) of an  $x_i \times x_i$  box (for simplified bond coordinates we use 45 degrees rotated lattice) and trace the hull until it reaches an edge. Bond values are calculated dynamically on the way (from a simple boolean random generator for the uncorrelated percolation). We reject hulls that make a loop and so don't reach an edge. Various hull properties are counted (for  $\mathcal{L}_{ij}$ ) and their cross-multiplications are calculated (for  $\Sigma_{ijk}$ ). This is repeated for millions of times for a single system size and the resulting data is aggregated. Finally,  $\mathcal{L}_{ij}$  and  $\Sigma_{ijk}$  are calculated.

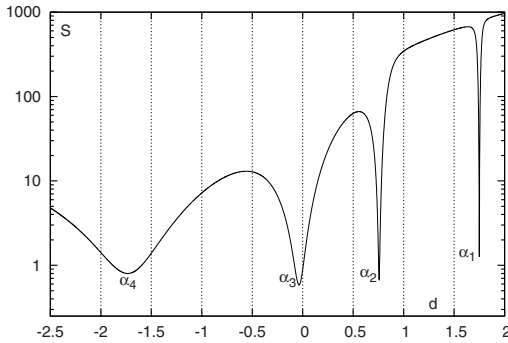


**Fig. 5.** A sample uncorrelated percolation hull exponent fitting function  $S(d)$  using four different properties ( $m = 4$ ) of the percolation cluster hull (twos, segs, sides, ends). The dips in the graph correspond to the exponents in (6). For this particular example, they are  $\alpha_1 = 1.7494 \pm 0.0019$ ,  $\alpha_2 = 0.756 \pm 0.018$ ,  $\alpha_3 = -0.04 \pm 0.16$  and  $\alpha_4 = -1.73 \pm 0.75$ .

finite-size correction terms to the error (systematic error), it may at the same time slightly increase the purely statistical uncertainty of the results.

We can now compare the results from using the simple model (Eq. (3)) against the one with  $m$  different properties (Eq. (6)). Results can be seen in Table 1. The method offers correct results (within the confines of the statistical

**Table 1.** Results comparing fitting to the simple model (3) versus the novel method ( $\Delta d_H$  is the difference between the calculated and the known value). Only first 6 data points at 8, 16, ..., 256 are used. LSQ  $N$  – regular least squares fitting against model (3) with one hull property and  $N$  system sizes. MLSQ  $M$  – method described in this paper, with  $M$  different hull properties and  $M + 2$  system sizes (as  $M$  increases so does the system's degrees of freedom, hence the uncertainty grows). Uncertainties are given with 0.95 confidence. Note that none of the LSQ results passed the chi-square test. The novel method offers consistent and accurate results.

	Name	Smallest $\Delta d_H$	Largest $\Delta d_H$
1	LSQ 3	$1.7299 \pm 0.0066$	$1.653 \pm 0.031$
2	LSQ 4	$1.720 \pm 0.011$	$1.619 \pm 0.044$
3	MLSQ 2	$1.7491 \pm 0.0011$	$1.7488 \pm 0.0011$
4	MLSQ 3	$1.7492 \pm 0.0017$	$1.7492 \pm 0.0017$
5	MLSQ 4	$1.7494 \pm 0.0019$	$1.7492 \pm 0.0018$

uncertainty), high precision (small uncertainty) and consistent results (each accepted  $S(d)$ , that is each combination of hull properties, yields similar results).

To be fair the gathered data is actually unusable for the simple model. This is due to the finite-size correction terms. To make use of the simple model (3), we would have to gather data at much larger system sizes. To reach similar results (low statistical error) to the novel method would demand vastly greater computational costs.

Aside from the scaling exponent of the hull, we have also tested the method to calculate the exponents of the unscreened perimeter  $d_U = 4/3$  and the cluster  $d_C = 91/48$  and obtained similar results to what has been demonstrated above; the novel algorithm performed flawlessly for all the cases. Finally, we have also studied the case of correlated percolation, when the scaling exponents depend on the roughness (Hurst) exponent  $H$ , so that  $d_H = d_H(H)$ . It is analytically known that  $d_H(0) = 1.5$  [12]; we have used our method to recover this result with a high degree of precision [13].

In earlier studies [7,14,15], the correction term exponents have been conjectured theoretically. When compared to these studies, our results confirm the presence of the simple correction terms (resulting from how we determine the diameter of a cluster and also from constant offsets to the measurements of hull properties). The inherent correction exponents described in those papers attributed to percolation cluster scaling have not been found here. The most likely explanation is that they were statistically insignificant.

## 6 Conclusion

A novel and universal method of determining the scaling exponents via finite-size Monte-Carlo simulations has been devised<sup>1</sup>. The method can be applied, if it is possible to find  $m \geq 2$  distinct quantities with equal asymptotic

<sup>1</sup> An implementation can be found at <https://code.google.com/p/perc2/>, see the 'calc' utility.

scaling exponents. The basic idea is to exploit the equality of the exponents of finite-size correction terms within the different physical quantities.

As an example, we have used the method to find the scaling exponents of the uncorrelated percolation cluster hulls. Here, the method offered consistent results and increased the accuracy of the scaling exponent estimates. The method has also been used previously in various contexts in the field with good results (cf. Refs. [5,13]).

The method is particularly useful when the convergence to the asymptotic scaling law is slow as it vastly reduces computational costs compared to traditional methods. We can make use of small system sizes that with traditional methods yield erroneous results or fail altogether. Also, the method is extremely useful, if it is necessary to find the exponents of the finite-size correction terms.

This work was supported by Estonian Science Foundation Grant No. 7909, Estonian Science Targeted Project No. SF0140077s08, and EU Regional Development Fund Centre of Excellence TK124.

## References

1. M.N. Barber, in *Phase Transitions and Critical Phenomena*, edited by C. Domb, J.L. Lebowitz (Academic Press, New York, 1983), Vol. 8, pp. 146–268
2. K. Binder, Rep. Prog. Phys. **60**, 487 (1997)
3. *Finite Size Scaling and Numerical Simulation of Statistical Systems*, edited by V. Privman (World Scientific, Singapore, 1990)
4. J. Kalda, Physica A **246**, 646 (1997)
5. J. Kalda, Europhys. Lett. **84**, 46003 (2008)
6. R. Bischof, P.R. Crompton, J. Exp. Theor. Phys. Lett. **84**, 729 (2006)
7. R.M. Ziff, Phys. Rev. E **83**, 020107 (2011)
8. J. Schmittbuhl, A. Hansen, H. Auradou, K.J. Måløy, Phys. Rev. E **61**, 3985 (2000)
9. A.B. Harris, J. Phys. C **7**, 1671 (1974)
10. H. Saleur, B. Duplantier, Phys. Rev. Lett. **58**, 2325 (1987)
11. M.B. Isichenko, Rev. Mod. Phys. **64**, 961 (1992)
12. J. Kondev, C.L. Henley, Phys. Rev. Lett. **74**, 4580 (1995)
13. I. Mandre, J. Kalda, Eur. Phys. J. B **83**, 107 (2011)
14. A. Aharony, J. Asikainen, Fractals **11**, 3 (2003)
15. J. Asikainen, A. Aharony, B.B. Mandelbrot, E.M. Rauch, J.P. Hovi, Eur. Phys. J. B **34**, 479 (2003)

PUBLICATION III

I. Mandre, J. Kalda. Intersections of moving fractal sets. *EPL (Europhysics Letters)*, 103(1):10012 (2013).



# Intersections of moving fractal sets

I. MANDRE and J. KALDA

*Institute of Cybernetics at the Tallinn University of Technology - Akadeemia tee 21, 12618, Tallinn, Estonia, EU*

received 15 May 2013; accepted 2 July 2013  
published online 26 July 2013

PACS 05.45.Df – Fractals  
PACS 05.40.Jc – Brownian motion  
PACS 05.45.Tp – Time series analysis

**Abstract** – Intersection of a random fractal or self-affine set with a linear manifold or another fractal set is studied, assuming that one of the sets is in a translational motion with respect to the other. It is shown that the mass of such an intersection is a self-affine function of the relative position of the two sets. The corresponding Hurst exponent  $h$  is a function of the scaling exponents of the intersecting sets. A generic expression for  $h$  is provided, and its proof is offered for two cases — intersection of a self-affine curve with a line, and of two fractal sets. The analytical results are tested using Monte Carlo simulations.

Copyright © EPLA, 2013

There is a wide spectrum of problems which can be reduced to finding and studying intersections of fractal sets. For instance, rain intensity is a multifractal function of space and time [1,2]; rainfall at a given point on Earth’s surface is a time-integral of this function — a measure of the intersection of the rain intensity field with a line, parallel to the time axis. Next, the Doppler absorption spectra depend on how many points of the flow move with a certain velocity in a certain direction; in the case of fully turbulent flows, velocity is a self-affine function of coordinates: the problem is reduced to finding the number of intersection points of a self-affine curve and a straight line. Further, it has been shown that silicate clay deposits, when drying, collapse into a self-affine surface; in the case of fractal deposits, the dry surface height is defined by the size of the intersection of the fractal with a vertical line [3].

While the list of examples could be further extended, we stop after providing just one more example which is discussed in more detail: reflection of light from surfaces with non-smooth gradients. More specifically, we consider surfaces with fractional Brownian (fB) gradient components; an example of such surfaces is provided by a free water surface in the case of fully developed wave turbulence [4,5].

Suppose a collimated beam of light falls onto a two-dimensional surface described by its height  $z = z(x, y)$ , such that the gradient components  $\partial_x z = f(x, y)$  and  $\partial_y z = g(x, y)$  are fB functions, so that

$$\langle [f(x, y) - f(x', y')]^2 \rangle \propto [(x - x')^2 + (y - y')^2]^H, \quad (1)$$

and the same scaling law holds for  $g(x, y)$ . Here, angular braces denote averaging over an ensemble of surfaces, and  $H$  is the Hurst exponent,  $0 < H < 1$ . Let us assume that the lower cut-off scale of this scaling law is unity, and that the gradient components become smooth below that scale. Furthermore, we assume that the wavelength of the incident light is much smaller than one. The functions  $f$  and  $g$  define a two-dimensional random self-affine surface (the gradient surface)  $u = f(x, y)$ ,  $v = g(x, y)$  in four-dimensional space  $x, y, u, v$ . The propagation direction of incident light from a point on the surface  $z$  is determined by its gradient components at that point. Therefore, the intensity of light reflected at a given direction from the entire surface  $z$  is proportional to the number of intersection points  $N$  of the gradient surface with a two-dimensional linear manifold  $u = u_0, v = v_0$ . This number is a random function of the propagation direction,  $N = N(u, v)$  — the light intensity fluctuates as the observation direction is changed. We will show that the function  $N(u, v)$  can be described by another Hurst exponent  $h = h(H)$ :

$$\langle [N(u, v) - N(u', v')]^2 \rangle \propto [(u - u')^2 + (v - v')^2]^h. \quad (2)$$

We start by deriving the dependance  $h = h(H)$  for the case of a fB curve intersecting with a line in two-dimensional space. Let us consider a finite-length segment  $x \in [0, L]$  of a fB curve  $u = f(x)$  with zero mean. Then, typically, the curve varies from  $u \sim -L^H$  to  $u \sim L^H$  (here “ $\sim$ ” means “is of the order of”). The fractal dimension of the fB curve is  $2 - H$  [6], and the dimension of its

intersection with a line  $u = u_0$  is  $d_f = 1 - H$  [7,8]. The intersection at level  $u = 0$  is also known as the zero set.

Since the lower cut-off scale is unity, the number of intersection points at some fixed  $u_0$  is estimated as  $N(u_0) \sim L^{d_f} = L^{1-H}$ . Let us denote the change in the number of intersection points when changing from “altitude”  $u_0$  to  $u_0 + \Delta u$  as  $\Delta N(\Delta u) \equiv N(u_0) - N(u_0 + \Delta u)$ . We now make use of a scale-decomposition of the function  $f(x)$  by introducing coarse-grained functions  $F_a(x) = \sum_{2^i \geq a} f_{2^i}(x)$ , where  $f_{2^i}(x)$  are the scale components that can be obtained, for instance, via a forward and reverse Fourier transform of  $f(x)$ , where only the wavelengths between  $2^{i-1}$  and  $2^i$  are kept. Let us denote the number of intersection points of the line  $u = u_0$  with the coarse-grained curve  $u = F_a(x)$  as  $N_a(u_0) \sim (L/a)^{1-H}$  and the change in the intersection points due to displacement  $\Delta u$  as  $\Delta N_a(\Delta u) \equiv N_a(u_0) - N_a(u_0 + \Delta u)$ . As we increase the level difference  $\Delta u$ , the line  $u = u_0 + \Delta u$  will cross from time to time the extrema of the function  $u = F_a(x)$ . By each crossing, the number of intersections  $N_a(u_0 + \Delta u)$  will change by two —increase in the case of a minimum, and decrease in the case of a maximum. When  $\Delta u \ll a^H$ , that is it is well below the vertical characteristic scale, these changes are purely incidental — they are caused by uncorrelated extrema that are separated by large distances. Therefore, at  $\Delta u \ll a^H$ , the value  $\Delta N_a(\Delta u)$  is a compound Poisson process, that is  $\Delta N_a(\Delta u) = \sum_{i=1}^{P(\Delta u)} D_i$ , where  $\{P(\Delta u) : \Delta u \geq 0\}$  is a Poisson process with rate  $\lambda$ , and  $\{D_i : i \geq 1\}$  are independent random values drawn with equal probability from  $\{-2, +2\}$ . The variance of the compound Poisson process [9] is  $\lambda \Delta u \langle D^2 \rangle$ ; but as  $\Delta N_a(\Delta u)$  has zero mean, we conclude that

$$\langle \Delta N_a(\Delta u)^2 \rangle = 4\lambda \Delta u \quad (\Delta u \ll a^H). \quad (3)$$

We estimate the density of extrema for  $N_a$  as  $\lambda \sim (L/a)/L^H = L^{1-H}a^{-1}$  —the number of peaks is  $L/a$  and they are distributed quasi-homogeneously in the range  $-L^H$  to  $L^H$ . We note that eq. (3) can also be used to estimate the scaling exponent for displacements below the lower cut-off scale of  $f(x)$ , that is for  $\Delta u \ll 1$ , we obtain a super-universality  $h(H) = 1/2$ .

Around each intersection point with the coarse-grained curve, the line  $u = u_0$  also intersects with the fine-scaled structure  $f(x) - F_a(x)$ . But as the intersection points with the coarse-grained curve are typically spaced at greater distances than  $a$ , the number of intersections with the fine-scaled structure around each such point are uncorrelated (as correlations in the fine-scaled structure only extend to distances around  $a$ ). We denote the average number of such intersections around each point as  $n_a \sim a^{1-H}$  and conclude that the total number of intersections with the whole curve  $u = f(x)$  is  $N(u_0) \sim n_a N_a(u_0) \sim a^{1-H} N_a(u_0)$ . As we move the intersecting line from level  $u_0$  to  $u_0 + \Delta u$ , the number of intersections with  $u = f(x)$  changes. When the displacement  $\Delta u$  is smaller than  $a^H$ , the contributions from the fine-scaled

intersections are highly correlated, but at displacement  $\Delta u \gg a^H$  they are basically uncorrelated. Consequently,

$$\Delta N(\Delta u) \sim a^{1-H} \Delta N_a(\Delta u) \quad (\Delta u \gg a^H). \quad (4)$$

At the marginally applicable limit  $\Delta u = a^H$ , eqs. (3) and (4) combine into

$$|\Delta N(a^H)| \sim a^{1-H} |\Delta N_a(a^H)| \sim L^{\frac{1-H}{2}} a^{\frac{1-H}{2}}. \quad (5)$$

To estimate  $|\Delta N(\Delta u)|$ , we choose  $a = \Delta u^{1/H}$ , yielding

$$|\Delta N(\Delta u)| \sim L^{\frac{1-H}{2}} \Delta u^{\frac{1-H}{2H}}, \quad (6)$$

and so the scaling exponent  $h$  for the intersection of a fB curve and a moving line is

$$h = \frac{1-H}{2H} \quad (1 \ll \Delta u \ll L^H). \quad (7)$$

It should be noted that for  $H < \frac{1}{3}$ , this equation yields  $h > 1$ . Result  $h > 1$  means that large-scale fluctuations are so strong that the gradients of large-scale components dominate over the gradients caused by small-scale fluctuations. In that case, eq. (2) would yield the Hurst exponent  $h = 1$ . However, using wavelet or Fourier analysis, it is possible to generalize eq. (2) and reveal scaling laws with  $h > 1$ .

Returning to the case of the intensity of light reflected by the sea surface, where we have an intersection of a self-affine surface and a flat surface in 4D space, the scaling law (2) can be derived in a similar fashion, resulting in  $h = \frac{2-2H}{2H}$ , where  $2 - 2H$  is the fractal dimension of the intersection studied.

We have run a series of Monte Carlo simulations to test the result (7). At each calculation point  $H$  we generated 1000 fractional Brownian curves  $f(x)$  with length  $L = 2^{27}$  [10–12]. Samples of the intersection functions  $N(u)$  can be seen in fig. 1. The data was analyzed using the continuous wavelet transform and the Mexican hat wavelet [13]. The results follow the predicted relationship  $h = \frac{1-H}{2H}$  quite closely except at greater values of  $H$  (fig. 1(d)). The discrepancy is due to distortions in the function  $N(u)$  —as  $L^H$  grows, the density of intersections falls and the function  $N(u)$  starts to experience large ranges where it is of constant small value (see fig. 1(c) for a sample  $N(u)$  at  $H = 0.7$ ). This is a finite-size effect —to overcome it one would have to calculate at much greater length  $L$ . We also did some calculations for  $H < 1/3$ . The results were as expected with  $h > 1$ .

We now turn our attention to general statistically self-similar fractal sets. It is easy to imagine that the interactions (changes in the intersection) of a line and a random fractal set at displacements well below the lower scaling length of the fractal are completely random. We have also found, that for the intersections of a fB curve or surface with a line or a plane, the analytically derived scaling exponents all came out as  $h = d_f/(2H)$ , where  $d_f$  is the

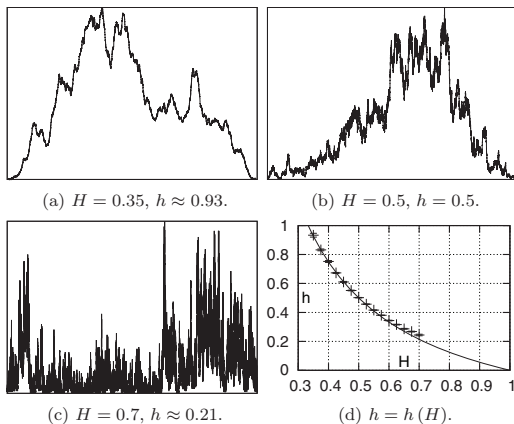


Fig. 1: (a)–(c): sample functions of  $N(u)$  for various  $H$ ; (d) Monte Carlo results for the scaling of the intersection of a fractional Brownian curve and a moving line, solid line is the predicted value.

fractal dimension of the intersection. Considering all this, one can conjecture that this relation also applies to intersections of general random fractals. We proceed to make this claim more specific.

Let us have two fractal sets  $\mathcal{F}$  and  $\mathcal{X}$  with corresponding fractal dimensions  $d_{\mathcal{F}}$  and  $d_{\mathcal{X}}$ . Let the set  $\mathcal{X}$  be translatable in some direction  $\hat{\mathbf{u}}$ , with the position identified by coordinate  $u$ . Further, we assume that it is self-similar and with finite scaling range  $[1, L]$ . This set may also have a topological dimension that is equal to its fractal dimension (for example, it may be a simple line or a plane). We assume that the fractal set  $\mathcal{F}$  is random, that is it is only statistically self-similar (we will clarify the nature of this randomness further along the way). Let the fractal  $\mathcal{F}$  have the same scaling range as  $\mathcal{X}$  in the directions perpendicular to  $\hat{\mathbf{u}}$  but let it be possibly self-affine in the direction  $\hat{\mathbf{u}}$  with scaling range  $[1, L^{H_{\hat{\mathbf{u}}}}]$ .

We denote the fractal dimension of the intersection of the two sets as  $d_f$  (for many cases  $d_f = d_{\mathcal{F}} + d_{\mathcal{X}} - D$ , where  $D$  is the dimension of the surrounding space). As the set  $\mathcal{X}$  moves, the total fractal mass of this intersection  $M(u)$  (the number of points, the surface area, the volume, or other such measure that is suitable for the given fractal depending on its topological dimension) will change. We fix  $u = u_0$  and denote this change at translation to  $u = u_0 + \Delta u$  as  $\Delta M(\Delta u) \equiv M(u_0) - M(u_0 + \Delta u)$ . We conjecture that the function  $M(u)$  is fractional-Brownian-motion-like, that is it can be described by

$$\langle \Delta M(\Delta u)^2 \rangle \propto |\Delta u|^{2h}, \quad (8)$$

with the Hurst exponent  $h$  as

$$h = \frac{d_f}{2H_{\hat{\mathbf{u}}}}, \quad (9)$$

where  $H_{\hat{\mathbf{u}}}$  describes the scaling of the fractal  $\mathcal{F}$  in the direction  $\hat{\mathbf{u}}$  ( $H_{\hat{\mathbf{u}}}$  is unity for a self-similar fractal set).

We will now continue with a derivation leading to this result for the case of self-similar fractals (with  $H_{\hat{\mathbf{u}}} = 1$ ). For this we will first approximate the fractals by the use of a ball cover —this results in a “coarse-grained” version of the fractal at a specific grain size. Then, we will derive how  $M(u)$  scales at movements either much smaller or much greater than the length used at the ball cover. Finally, we bring these two estimates together to yield the exponent  $h$ .

In case the set  $\mathcal{F}$  is self-similar, the fractal mass of the intersection  $\mathcal{F} \cap \mathcal{X}$  can be estimated as  $M(u_0) \sim L^{d_f}$ , where  $d_f = d_{\mathcal{F}} + d_{\mathcal{X}} - D$ . Let us assume that we can find minimal covers for both sets  $\mathcal{F}$  and  $\mathcal{X}$  with  $D$ -dimensional closed balls of diameter  $a$ , where  $1 \ll a \ll L$ . The number of balls in either cover can be estimated as  $N_{\mathcal{F}}(a) \sim (L/a)^{d_{\mathcal{F}}}$  and  $N_{\mathcal{X}}(a) \sim (L/a)^{d_{\mathcal{X}}}$ .

At a location where two balls, each from a different set, intersect, the fractal sets themselves usually intersect, with the average fractal mass of the intersection (assuming  $\mathcal{F}$  is random, for example the balls can’t be globally aligned) estimated as  $m_a \sim a^{d_f}$ . The total number of such intersections is  $N_a(u_0) \sim M(u_0)/m_a \sim (L/a)^{d_f}$ . We move the set  $\mathcal{X}$  in the direction  $\hat{\mathbf{u}}$  by distance  $\Delta u$ . This will cause the cover of the set  $\mathcal{X}$  also move. As a ball from that cover moves, it penetrates or exits balls covering the standing set  $\mathcal{F}$ . As a result, the value  $N_a(u_0)$  will increase or decrease by one. We denote the total change in the number of intersecting balls as  $\Delta N_a(\Delta u) \equiv N_a(u_0) - N_a(u_0 + \Delta u)$ .

In case the movement is much greater than  $a$ , that is  $a \ll \Delta u \ll L$ , a moving ball that is penetrating a standing ball will exit it. We assume that  $\mathcal{F}$  is random in such a way that the masses of the sub-fractals contained in individual standing balls separated by distances much greater than  $a$  are uncorrelated. In such a case

$$\Delta M(\Delta u) \sim m_a \Delta N_a(\Delta u) \quad (a \ll \Delta u \ll L). \quad (10)$$

In case the movement is much smaller than  $a$ , that is  $\Delta u \ll a$ , a moving ball that is intersecting a standing ball will rarely exit it. Also, it has very little chance to interact with other standing balls or the correlations in their placement (defined by the structure of the fractal). With small movement individual moving balls have no chance to interact with the fractal structure of the ball cover. And assuming the fractal  $\mathcal{F}$  is random, that is the balls are not globally aligned, we can ignore their interactions as a group. In such a case the change in the number of balls intersected can be approximated as a compound Poisson process, that is  $\Delta N_a(\Delta u) = \sum_{i=1}^{P(\Delta u)} D_i$ , where  $\{P(\Delta u) : \Delta u \geq 0\}$  is a Poisson process with rate  $\lambda$ , and  $\{D_i : i \geq 1\}$  are independent random values drawn with equal probability from  $\{-1, +1\}$ . The variance of the compound Poisson process is  $\lambda \Delta u \langle D^2 \rangle$ ; but as  $\Delta N_a(\Delta u)$  has zero mean, we conclude that

$$\langle \Delta N_a(\Delta u)^2 \rangle = \lambda \Delta u \quad (\Delta u \ll a). \quad (11)$$

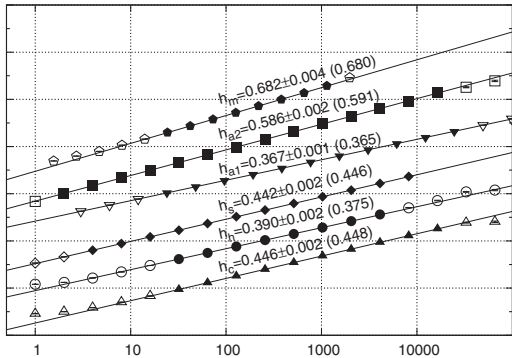


Fig. 2: Wavelet based scaling exponent fitting for the intersections of random percolation cluster ( $h_c$ ) and hull ( $h_h$ ); the randomized Sierpiński carpet ( $h_s$ ); the self-affine randomized Sierpiński carpet ( $h_{a1}$  and  $h_{a2}$ ); and the intersection of a percolation cluster with a deterministic Sierpiński carpet ( $h_m$ ). Results for different fractals have been moved up or down to fit on the same graph. Uncertainties are given with 0.95 significance. The predicted values  $h = d_f / (2H)$  are in parentheses. Only filled points were used for the fits.

We now estimate the Poisson process rate  $\lambda$ . At displacement  $\Delta u$  the moving balls cover the volume  $V_{\mathcal{X}} \sim N_{\mathcal{X}}(a)a^{D-1}\Delta u \sim L^{d_{\mathcal{X}}}a^{D-1-d_{\mathcal{X}}}\Delta u$ . Assuming the standing balls are distributed quasi-homogeneously (the fractal  $\mathcal{F}$  is random), their density per volume of space is  $\rho_{\mathcal{F}} \sim N_{\mathcal{F}}(a)/L^D \sim L^{d_{\mathcal{F}}-D}a^{-d_{\mathcal{F}}}$ . The number of balls encountered during movement  $\Delta u$  must then be  $N_{\Delta u} \sim \rho_{\mathcal{F}}V_{\mathcal{X}} \sim L^{d_{\mathcal{F}}}a^{-1-d_{\mathcal{F}}}\Delta u$ . The rate of balls encountered is  $\lambda \sim N_{\Delta u}/\Delta u \sim L^{d_{\mathcal{F}}}a^{-1-d_{\mathcal{F}}}$ .

At the marginally applicable limit  $\Delta u = a$  of the two expressions (10) and (11), we estimate the change in the mass as

$$|\Delta M(a)| \sim m_a \sqrt{\lambda} a^{1/2} \sim L^{d_f/2} a^{d_f/2}. \quad (12)$$

Since the ball cover size  $a$  can be freely chosen between 1 and  $L$ , we can pick  $a = \Delta u$ , confirming conjecture (8) with the Hurst exponent  $h = d_f/2$ .

For the case  $H_{\hat{\mathbf{u}}} \neq 1$ , one would have to take into account that the correlations in the self-similar structure of the fractal scale at a different rate in the direction  $\hat{\mathbf{u}}$ .

The intersection of two fractals may have a dimension less than 0. Previously, it has been interpreted as how “empty” the intersection is [8,14]. In eq. (9) this would result in negative  $h$ . This is not necessarily a pathological case, as a negative  $h$  can be used when instead of (8) the scaling is given through the Fourier power spectrum, that is through the relation  $\langle |\psi_{\mathbf{k}}|^2 \rangle \propto |\mathbf{k}|^{-2h-1}$ . However, we have not tested this numerically.

To test the relation (9) we ran Monte Carlo simulations for the following cases: two-dimensional random bond percolation cluster and hull intersected with a horizontal line, with predicted  $h_c = (91/48 + 1 - 2)/2$  and

$h_h = (7/4 + 1 - 2)/2$  for the cluster and hull respectively; randomized  $3 \times 3$  Sierpiński carpet [15–19] (with one cell cleared randomly at each construction step) intersected with a horizontal line, with predicted  $h_s = (\log_3 8 + 1 - 2)/2$ ; self-affine randomized  $4 \times 3$  Sierpiński carpet (with one cell cleared randomly at each construction step) intersected with vertical and horizontal lines, with the carpet’s box dimension  $d_{4 \times 3} = \log_3(3^{1-\log_4 3} 11^{\log_4 3})$  and predicted scaling exponents  $h_{a1} = \frac{\log_4 11/4}{2 \log_3 4}$  and  $h_{a2} = \frac{d_{4 \times 3} + 1 - 2}{2 \log_4 3}$ ; percolation cluster intersected with a deterministic  $3 \times 3$  Sierpiński carpet, with predicted  $h_m = (91/48 + \log_3 5 - 2)/2$ . The results from the Monte Carlo simulations are all very close to the predicted values (fig. 2). As we increased calculation lattice sizes we saw improvement across the board, indicating that the small discrepancies are due to the finite size effects.

To conclude, it is now easy to see that the flow rate of the river Nile, famously studied by Harold Edwin Hurst [20], is an integral quantity of the fractal structure of precipitation [1,2] over its drainage basin, and as confirmed by the analytical relation we have found, is self-affine. This analytical relation should be applicable in both predictive and descriptive capacity for many problems, from the matter distribution of the universe to the formation of  $1/f$ -like noise in semiconductor devices.

\*\*\*

This work was supported by Estonian Science Targeted Project No. SF0140077s08, and EU Regional Development Fund Centre of Excellence TK124. The authors would like to thank the Department of Computer Engineering at the Tallinn University of Technology for providing computational resources.

## REFERENCES

- [1] LOVEJOY S. and MANDELBROT B. B., *Tellus A*, **37A** (1985) 209.
- [2] LOVEJOY S. and SCHERTZER D., *J. Geophys. Res.*, **95** (1990) 2021.
- [3] FOSSUM J. O., BERGENE H. H., HANSEN A., O’ROURKE B. and MANIFICAT G., *Phys. Rev. E*, **69** (2004) 036108.
- [4] ZAKHAROV V. E. and FILONENKO N. N., *J. Appl. Mech. Tech. Phys.*, **8** (1967) 37.
- [5] YACHENKO A. I., KOROTKEVICH A. O. and ZAKHAROV V. E., *Phys. Rev. Lett.*, **92** (2004) 134501.
- [6] OREY S., *Z. Wahrscheinlichkeitstheor. Verw. Geb.*, **15** (1970) 249.
- [7] MANDELBROT B. B., *The Fractal Geometry of Nature* (Freeman, New York) 1982.
- [8] MANDELBROT B. B., *J. Stat. Phys.*, **34** (1984) 895.
- [9] TILMS H. C., *A First Course in Stochastic Models* (John Wiley & Sons Ltd., Chichester, UK) 2003.
- [10] DAVIES R. B. and HARTE D. S., *Biometrika*, **74** (1987) 95.
- [11] DIETRICH C. R. and NEWSAM G. N., *SIAM J. Sci. Comput.*, **18** (1997) 1088.

- [12] WOOD A. T. A. and CHAN G., *J. Comput. Graph. Stat.*, **3** (1994) 409.
- [13] SIMONSEN I., HANSEN A. and NES O. M., *Phys. Rev. E*, **58** (1998) 2779.
- [14] MANDELBROT B. B., *Physica A*, **163** (1990) 306.
- [15] SIERPIŃSKI W., *C. R. Acad. Sci. Paris*, **162** (1916) 629.
- [16] McMULLEN C., *Nagoya Math. J.*, **96** (1984) 1.
- [17] BEDFORD T. J., *Crinkly curves, Markov partitions and dimension*, PhD, University of Warwick (1984).
- [18] PERES Y., *Math. Proc. Cambridge Philos. Soc.*, **115** (1994) 437.
- [19] GUI Y. and LI W., *Nonlinearity*, **21** (2008) 1745.
- [20] HURST H. E., *Trans. Am. Soc. Civ. Eng.*, **116** (1951) 770.



---

## CURRICULUM VITAE

---

### PERSONAL DATA

Name	Indrek Mandre
Date and place of birth	22.02.1979, Tallinn, Estonia
Nationality	Estonian

### CONTACT INFORMATION

Address	Tallinn University of Technology, Department of Cybernetics, Akadeemia tee 21B, 12618 Tallinn, Estonia
Web	<a href="http://www.mare.ee/indrek/">http://www.mare.ee/indrek/</a>
Phone	+37256210348
E-mail	indrek(at)mare.ee

### EDUCATION

2008 – 2010	Tallinn University of Technology MSc cum laude, Engineering Physics / Applied Mathematics
1997 – 2001	Tallinn University of Technology BSc cum laude, Informatics

### LANGUAGE COMPETENCE

Estonian	native
English	fluent

## PROFESSIONAL EMPLOYMENT

2015 –	Starship Technologies, Senior Developer
2003 – 2008	Skype, Senior Developer
2000 – 2003	Trigger Software / TELE2, Web Developer

## DEFENDED THESES

- 2010, Fractal dimensions of correlated percolation, MSc, supervisor PhD Jaan Kalda, Tallinn University of Technology, Faculty of Science, Institute of Physics, Institute of Cybernetics
- 2001, PHP to Java translator, BSc, supervisor PhD Jaak Henno, Tallinn University of Technology, Faculty of Information Technology

## PUBLICATIONS

- I. Mandre, J. Kalda. Monte-Carlo study of scaling exponents of rough surfaces and correlated percolation. *The European Physical Journal B*, 83(1):107-113 (2011)
- I. Mandre, J. Kalda. Efficient method of finding scaling exponents from finite-size Monte-Carlo simulations. *The European Physical Journal B*, 86(2):56 (2013)
- I. Mandre, J. Kalda. Intersections of moving fractal sets. *EPL (Europhysics Letters)*, 103(1):10012 (2013)

## CONFERENCE PRESENTATIONS

- I. Mandre, J. Kalda. Intersections of moving fractal sets (poster). *STATPHYS 25, Seoul, Korea, 2013*

## PATENTS AND PATENT APPLICATIONS

- Communication system, US 8345581 B2
- Instant messaging activity notification, US 20080201438 A1
- Synchronising contacts, US 7743024 B2

- Method and system for delivering messages in a communication system, US 8275841 B2
- Method and system for autonomous or semi-autonomous delivery, WO2017064202
- Method, device and assembly for map generation, WO2017076928
- Device and method for autonomous localisation, WO2017076929
- Method and system for calibrating multiple cameras, WO2018046617

---

## ELULOOKIRJELDUS

---

### ISIKUANDMED

Nimi	Indrek Mandre
Sünniaeg ja -koht	22.02.1979, Tallinn, Eesti
Kodakondsus	Eesti

### KONTAKTANDMED

Aadress	Tallinna Tehnikaülikool, Küberneetika instituut, Akadeemia tee 21B, 12618 Tallinn, Eesti
Www	<a href="http://www.mare.ee/indrek/">http://www.mare.ee/indrek/</a>
Telefon	+37256210348
E-post	indrek(at)mare.ee

### HARIDUS

2008 – 2010	Tallinna Tehnikaülikool MSc cum laude, tehniline füüsika / rakendusmatemaatika
1997 – 2001	Tallinna Tehnikaülikool BSc cum laude, informaatika

### KEELTEOSKUS

eesti keel	emakeel
inglise keel	kõrgtase

## TEENISTUSKÄIK

2015 –	Starship Technologies, vanem arendaja
2003 – 2008	Skype, vanem arendaja
2000 – 2003	Trigger Software / TELE2, arendaja

## KAITSTUD LÕPUTÖÖD

- 2010, Fractal dimensions of correlated percolation, MSc, juhendaja PhD Jaan Kalda, Tallinna Tehnikaülikool, Matemaatika- ja loodusteaduskond, Küberneetika instituut
- 2001, PHP to Java translator, BSc, juhendaja PhD Jaak Henno, Tallinna Tehnikaülikool, Infotehnoloogia teaduskond

## AVALDATUD ARTIKLID

- I. Mandre, J. Kalda. Monte-Carlo study of scaling exponents of rough surfaces and correlated percolation. *The European Physical Journal B*, 83(1):107-113 (2011)
- I. Mandre, J. Kalda. Efficient method of finding scaling exponents from finite-size Monte-Carlo simulations. *The European Physical Journal B*, 86(2):56 (2013)
- I. Mandre, J. Kalda. Intersections of moving fractal sets. *EPL (Europhysics Letters)*, 103(1):10012 (2013)

## ETTEKANDED KONVERENTSIDEL

- I. Mandre, J. Kalda. Intersections of moving fractal sets (poster). *STATPHYS 25, Seoul, Korea, 2013*

## PATENDID JA PATENDITAOTLUSED

- Communication system, US 8345581 B2
- Instant messaging activity notification, US 20080201438 A1
- Synchronising contacts, US 7743024 B2

- Method and system for delivering messages in a communication system, US 8275841 B2
- Method and system for autonomous or semi-autonomous delivery, WO2017064202
- Method, device and assembly for map generation, WO2017076928
- Device and method for autonomous localisation, WO2017076929
- Method and system for calibrating multiple cameras, WO2018046617

